Automatic Esophageal Intubation Detection Using Giant Magneto Resistance Sensors

Bradley J. Alson

Thesis submitted to the faculty of the Virginia Polytechnic Institute and State University in partial fulfillment of the requirements for the degree of

Master of Science
In
Mechanical Engineering

Alfred L. Wicks
John P. Bird
Andre A. Muelenaer

July 2, 2015
Blacksburg, VA

Keywords: Airway Management, Intubation

Automatic Esophageal Intubation Detection Using Giant Magneto Resistance Sensors

Bradley J. Alson

ABSTRACT

This thesis will cover the principle, design, and construction of an automatic esophageal intubation detector. This device uses a giant magneto recitative sensor to and a magnetized stylet to automatically measure the position of an ET tube in a person's throat. This method is less subjective than currently used methods such as end tidal CO_2, as it does not rely on user interpretation of data or physiological state of the patient. The device developed during this project was tested on an anatomical mockup, a porcine airway model, and an intubation training dummy. In all three tests, the device performed well, accurately indicating tracheal intubation when the tube was placed in the trachea. Only one instance of a false positive indication of tracheal intubation was recorded and this occurred in an atypical and avoidable situation. As of now, the device functions in non-obese adult male patients, but plans are in place to increase usability for the entire population.

Acknowledgments

The author thanks the Virginia Tech Mechatronics Lab and the Pediatric Medical Device Institute at Virginia Tech for the for the use of lab space and equipment, Dr. Robertson and the Biomedical Engineering and Sciences department at Virginia Tech for providing materials for porcine model testing, and the Department of Emergency Medicine at Wake Forest University for the project proposal as well as testing assistance and feedback.

Table of Contents

List of Figures

List of Tables

Chapter 1. Introduction

Problem Overview and Definition

Establishment and maintenance of an airway is the first and arguably the most critical step in any form of emergency care. Without an established airway, all other subsequent life-saving steps become meaningless. There are many different ways to establish an airway and the method used is often dictated by the context in which care is being provided. Sometimes, establishing an airway is as easy as monitoring a patient who is breathing on their own. Other times, the severity of an injury requires more invasive methods. Determining which type of airway is needed is dictated by the condition of the patient and the predicted outcome of the current procedure [1].

When a patient cannot maintain their own airway, one of the main techniques used to establish an airway is endotracheal intubation. Endotracheal intubation establishes an airway by inserting a tube into the throat, past the vocal cords and into the trachea of a patient. While this is a conceptually simple procedure, the natural geometry of the throat along with other complications such as obstructions, swelling, or trauma can make this procedure much more difficult. Mastering intubation requires extensive training as well as constant practice in order to maintain the skills needed to be proficient at this procedure. This difficulty is compounded by the fact that intubation must often be performed under stressful situations or non-ideal settings. Mistakes happen and detecting them quickly is critical for a patient's health and well-being [1].

One common mistake, and the focus of this thesis, is esophageal intubation. Esophageal intubation is a case where the endotracheal tube is placed in the esophagus instead of the trachea. This can easily be corrected by backing out the tube and making another attempt at passing through the vocal cords. However, if this error remains undetected deadly complications can occur. First, ventilating a patient's stomach through the esophagus provides no oxygen to the patient's blood, leading to hypoxia and death. Ventilation of the stomach can also cause regurgitation and aspiration of gastric contents, further complicating the airway management process [2].

Because of the extremely serious nature of esophageal intubation, many different methods have been developed to attempt to detect it earlier or prevent it altogether. One method is end tidal CO_2, which looks for CO_2 being generated by the body during proper ventilation. Other rudimentary methods focus on visually confirming placement by observing passage of the cords,

or monitoring the rise and fall of the chest. While useful in detecting mistakes, most current methods look at physiological evidence or other qualitative indicators that the procedure has been performed correctly, and not direct observation of tube position. This problem along with operator inexperience or over-confidence leads to a small but significant number of undetected esophageal intubations[3].

Proposed Solution

This thesis seeks address the ambiguity in assessing tube position by providing a direct observation of an endotracheal tube in a patient. By doing this, many of the subjective components of the procedure are mitigated. Direct observation of tube position means that the procedure need not rely on operator interpretation, which is often clouded by inexperience or overconfidence. It also provides an assessment that is independent of the physical state of the patient. For example the end tidal CO_2 method fails when the patient is in cardiac arrest, as there is no CO_2 being generated by the lungs [1].

To achieve the goal of direct observation, this project implements an intubating magnetic stylet and a giant magneto resistive sensor to assess tube position in the neck. Because the trachea sits above the esophagus, an endotracheal tube in the trachea is much closer to the surface of the neck then one placed in the esophagus. By measuring this distance with a magnetic sensor, it is possible to determine whether a tube has been placed in the esophagus or the trachea during the intubation procedure. The feedback from the device is designed to be binary, providing a clear yes or no answer to the question of “Am I in the trachea?”. The device will also be able to perform these measurements in real time, unlike other assessment methods that require the tube to be in place before the location can be verified. This not only allows for a quantitative approach to assessing tube placement, but also allows for much faster reactions to mistakes, saving time and lives.

Project Scope and Goals

The primary scope of this project is to create a method for automatically assessing endotracheal tube placement and to construct a prototype to evaluate that method. The prototype device should accurately assess tube placement in a representative model of an adult male patient. The device does not seek to replace any current method in the airway management chain nor

change the way intubations are performed. Instead, it seeks to augment the procedure to add more quantitative assessments of airway placement. The current iteration of the device is solely focused on oral intubation and therefore will not test or address blind nasal intubation. Finally, the device is only designed to assess esophageal intubations and not other errors with intubation methods, such as right main stem intubation.

Several design goals must be met in order to achieve these objectives. First, the device must accurately evaluate whether or not an endotracheal tube has been placed in the trachea or the esophagus of a patient. This assessment should be based off direct observation of endotracheal tube placement, not the physiological state of the patient. In other words, the tubes position should be evaluated using anatomical properties, such as geometry or tissue composition. This helps avoid some of the problems with current detection methods that rely on user interpretation.

Next, the device should provide easy-to-interpret, non-subjective feedback to the user. While many of the current tools for assessing endotracheal tube placement are accurate, they often provide subjective feedback. It is then left to the EMT or doctor to decide whether this information is correct. These assessments are often clouded by inexperience or over-confidence causing the operator to mistrust their equipment. This, coupled with the fact that emergency medicine is a stressful environment, results in of misinterpretation of tube placement [4]. This design should provide a clear “yes or no” feedback to the user, making it much harder and less excusable for them to mistake the tube position.

The device should be able to perform this assessment in real time, providing information about tube position while the ET tube is being placed in the throat. Other methods for esophageal intubation assess tube position after the tube has been placed, increasing the time it takes to react to a mistake. Real time assessment provides feedback while the procedure is being performed allowing the EMT or doctors to react quickly to mistakes, giving them more time to establish an airway.

The next goal of the project is that the device should be accurate. Specifically, the device should never present a false positive indication of tracheal intubation. A false positive result can be deadly as it could lead the doctor or EMT to the false assumption that the procedure has been performed correctly. To avoid this, it is acceptable for the device to have a higher false negative rate, meaning the devices will fail safe in the event of an ambiguous or atypical result.

Next, the device should be easy to deploy in both the pre-hospital and emergency room settings. The device should be simple in both design and operation. The more complicated a device is to use, the more training required before it can be deployed. The device should not interfere with the current intubation procedure or any of the equipment being used to aid the patient. The device should also be inexpensive. This ensures that it can be deployed to a variety of locations, from rural hospitals to ambulances. One of the major problems with advanced tube assessment tools like video laryngoscope is the fact that a single unit can cost anywhere from $5000 to $25000[5].

Finally, the device must work in most typical adult patients. Because of its reliance on geometry, this device will be designed to work on average adult male patients. This iteration will focus on demonstrating the functionality of the detection methods with future iterations expanding the usability of the device. After the method is demonstrated in the adult male model, further research will be done to expand its functionality to work in adult female and pediatric patients.

Chapter 2. Literary Review and Background Information

Before beginning the discussion of intubation procedures and medical related design decisions, it is necessary to understand the basic anatomy of the system being researched. This section will contain diagrams and descriptions of the important anatomical features of the human throat and upper airway. The reader should take the time to familiarize themselves with these features and anatomical terms before reading subsequent sections.

Anatomy References

Figure 1 shows a cross section of the human upper airway. It consists of the mouth and nasal cavity along with pharynx and the upper part of the larynx. The pharynx is the space in the back of the throat from the nasal cavity to the entrance to the trachea and the esophagus. The larynx is the part of the airway that connects the pharynx to the lungs and consists of the epiglottis, the vocal cords, and the trachea.

The trachea is a ridged tube made of cartilage and connective tissue that connects the lungs to the pharynx. It sits in the front of the neck anterior to the esophagus. During respiration, air passes through the nose or mouth, through the pharynx, and into the trachea. The main goal of an intubation is to place an endotracheal tube securely in the trachea.

The next important anatomical feature is the esophagus. The esophagus is a soft muscular tube through which food passes during swallowing. It connects the stomach with the mouth and

upper airway and sits directly behind the trachea. Esophageal intubation occurs when an endotracheal tube is inserted into the esophagus instead of the trachea.

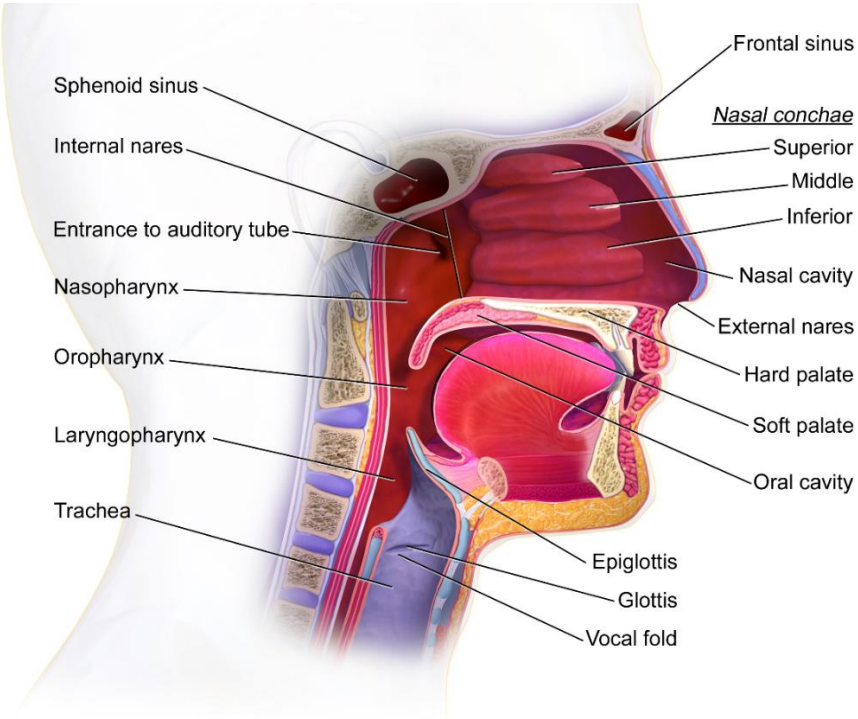

Figure 1. This figure shows a diagram of the upper airway with labels. The most important anatomical features for this paper are the trachea and the esophagus, as these are the two locations the sensor will try to differentiate between. The epiglottis and vocal fold (vocal cords) are also important as they act as landmarks during the intubation procedure.

"Blausen 0872 UpperRespiratorySystem" by BruceBlaus. Blausen.com staff. "Blausen gallery 2014". Wikiversity Journal of Medicine. DOI:10.15347/wjm/2014.010. ISSN 20018762. - Own work. Licensed under CC BY 3.0 via Wikimedia Commons, used with permission, 2015
https://commons.wikimedia.org/wiki/File:Blausen_0872_UpperRespiratorySystem.png#/media/File:Blausen_0872_UpperRespiratorySystem.png

Two other anatomical features of note are the vocal cords and epiglottis. These features are the primary landmarks that an EMT looks for and manipulates when performing an intubation. The epiglottis is a flexible piece of cartilage that sits above the vocal cords and opening to the trachea. During swallowing, the epiglottis covers the trachea to prevent food from entering. During the intubation procedure, the epiglottis is manipulated to reveal the vocal cords. By pulling the epiglottis forward or pressing on the super-glottic fold the vocal cords can be revealed, facilitating tube passage. The vocal cords are the primary target sought during intubation, as the fundamental way of assessing tube placement is by visualizing the passage of an ET tube through the cords. Figure 2 shows a diagram of the vocal cords and epiglottis as seen from above.

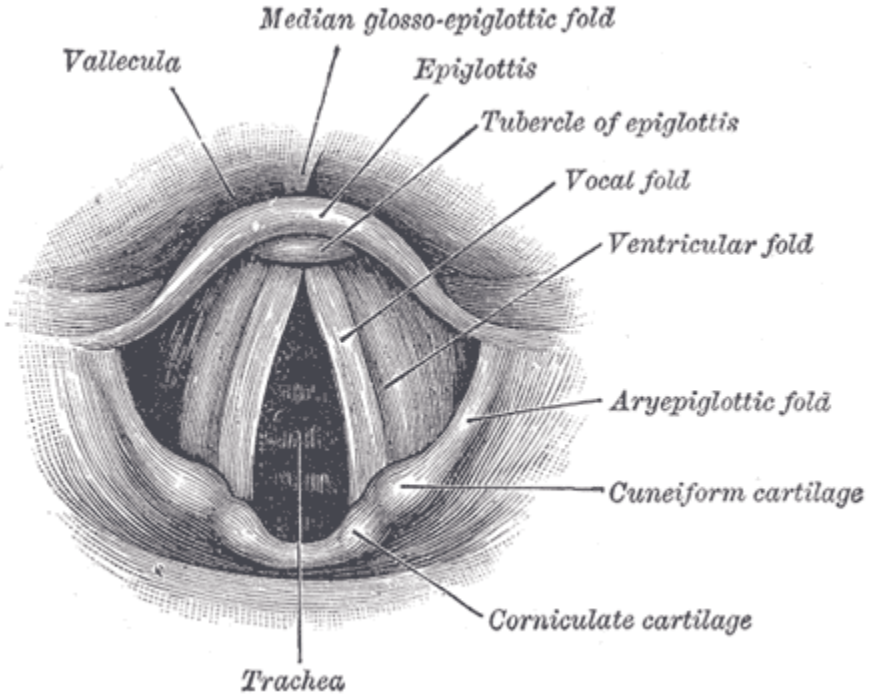

Figure 2. This figure shows diagram of the vocal cords and epiglottis as seen from above. The goal of an intubation procedure is to pass the ET tube through the vocal cords and into the trachea. During an intubation procedure, a doctor or EMT manipulates the epiglottis to allow for visualization of the vocal cords.

"Gray956" by Henry Vandyke Carter - Henry Gray (1918) Anatomy of the Human Body, Bartleby.com: Gray's Anatomy, Plate 956. Licensed under Public Domain via Wikimedia Commons, public domain, 2015

Figure 3 shows the external structure of the trachea. The main anatomical features to be identified in this figure are the median cricothyroid ligament and cricothyroid membrane. These structures provide anatomical landmarks that will be referenced later in the paper when discussing sensor position on neck.

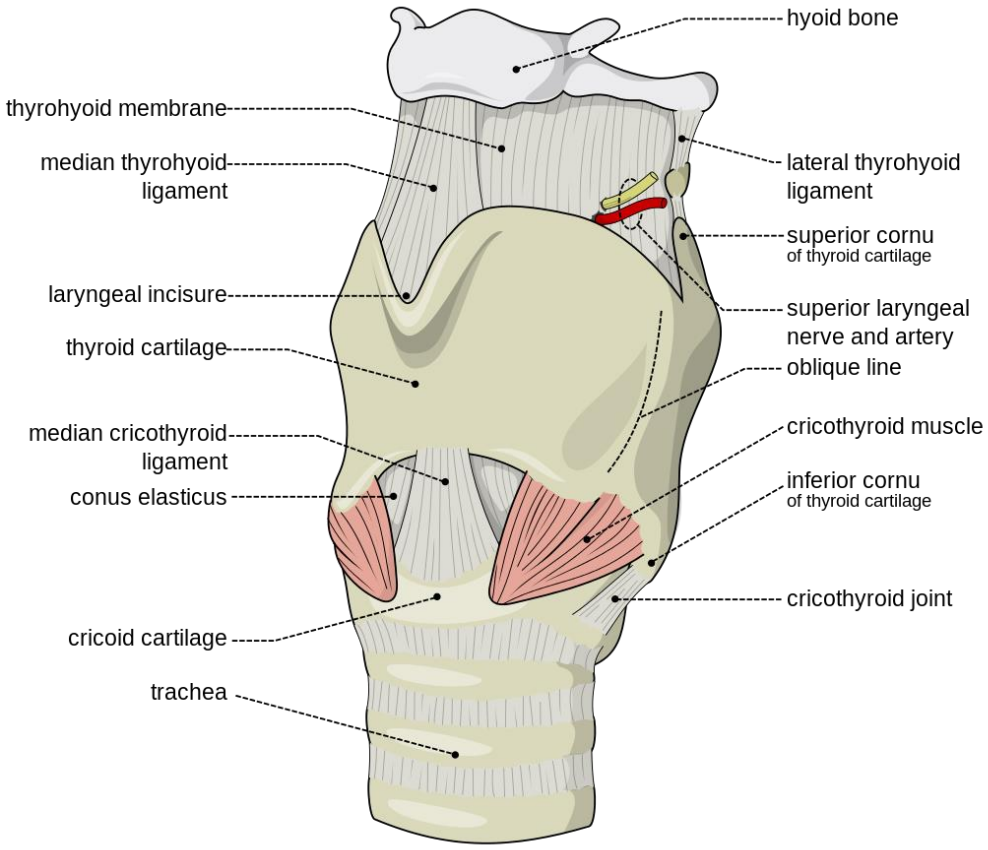

Figure 3. A diagram of the external anatomical features of trachea. Note the cricoid cartilage and median cricothyroid ligament. The cricoid cartilage and median cricoid membrane will serve as anatomical landmarks for sensor placement later in this paper.

"Larynx external en" by Olek Remesz (wiki-pl: Orem, commons: Orem) - Own work, modified SVG version of PD picture from Gray's Anatomy.. Licensed under CC BY-SA 2.5-2.0-1.0 via Wikimedia Commons, used with permission, 2015
https://commons.wikimedia.org/wiki/File:Gray956.png#/media/File:Gray956.png

General Concepts

This section will provide an overview of the intubation procedure, some of the fundamental tools used during intubation, and the methods for deciding when intubation is appropriate. Understanding these subjects is not only vital to development of a successful intubation detector, but also useful in establishing the scope of the project.

Intubation Definition

Intubation is an emergency medical procedure used to establish or maintain and airway in a patient who cannot do so on their own. It is a much less invasive method than a surgical airway

and provides a better airway than bag and mask ventilation alone. At its simplest, an intubation places a breathing tube in the trachea of the patient. This tube keeps the airway open in the event that the patient cannot do so on their own. This also ensures that air from a ventilator only enters the lungs and not the stomach, which can cause regurgitation of gastric contents. In most cases, the intubation tube also prevents aspiration of gastric contents by sealing the trachea with an inflatable balloon.

There are several primary indicators of intubation. First is the case when a patient cannot protect or maintain an airway. An example may be a patient with sever alcohol poisoning. The patient may still be able to breathe on his or her own but the effects of alcohol may cause them to aspirate gastric contents. The second case is when a patient cannot oxygenate effectively. In this case, the intubation is preformed to aid oxygenation not protect the airway [1] . This would be used in the event of a cardiac arrest, where the patient's airway is viable, but they cannot oxygenate because there is no blood flow. The final case in which intubation is necessary is when the patient's condition may deteriorate to the point where they cannot maintain an airway. One example would be a case of traumatic neck injury near the trachea. This patient may enter the ER with the ability to maintain their airway, but because of the damage to their trachea and throat, their airway could quickly become compromised.

Intubation Tools

There are numerous tools available to a doctor or EMT to help facilitate successful intubation, from fiber optic scopes to lighted stylets. While the tools available vary from department to department, there are a few notable tools found in every intubation kit. This section will provide an overview of these commonly used tools, as well as some specialized tools.

The first and most important tool is the endotracheal tube or ET tube as seen in Figure 4. This device is a disposable tube made of soft plastic, such as PVC. These tubes come in varying sizes to accommodate different patients. One end of the tube has a plastic connection point. This connector is a standard size and is designed to interface with both bag mask ventilators and mechanical ventilators. The other end of the tube has an inflatable balloon. This balloon inflates with air through a small tube and valve assembly. The balloon helps keep the endotracheal tube in the throat and prevents aspiration of foreign material during the procedure. The tube itself has depth markings on the side to help EMTs and doctors assess insertion depth of the tube[1].

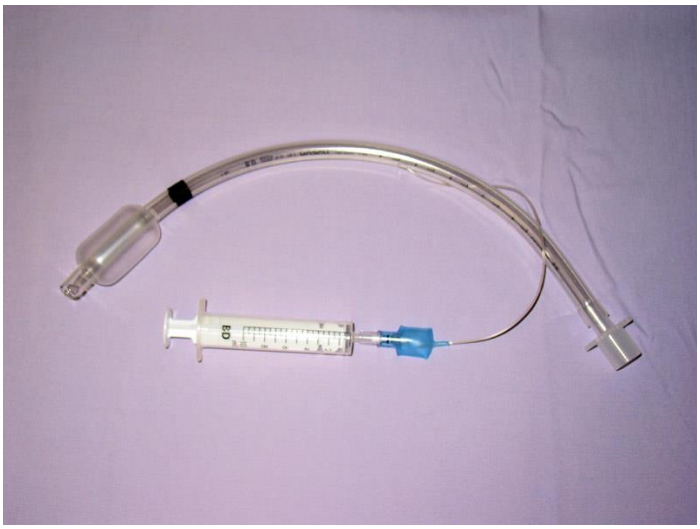

Figure 4. An ET tube with an inflatable cuff(left). Tubes are made of PVC or other flexable plastics and come in a variety of diameters. The inflatable cuff is used to secure the tube in the throat and shield the airway from gastirc contents.

"Sondeintubation" by bigomar2 - Self-photographed. Licensed under CC BY-SA 3.0 via Wikimedia Commons, used with permission, 2015
https://commons.wikimedia.org/wiki/File:Sondeintubation.jpg#/media/File:Sondeintubation.jpg

Along with the intubation tube, an EMT or doctor often uses an intubating stylet to assist with the procedure. This stylet is a flexible aluminum or steel wire coated in plastic, which is placed inside the ET tube during the intubation procedure. An example stylet is shown in Figure 5. It is used to provide support to the tube while being pushed by the EMT or doctor. It also makes it easier to guide the tube into the right location[1].

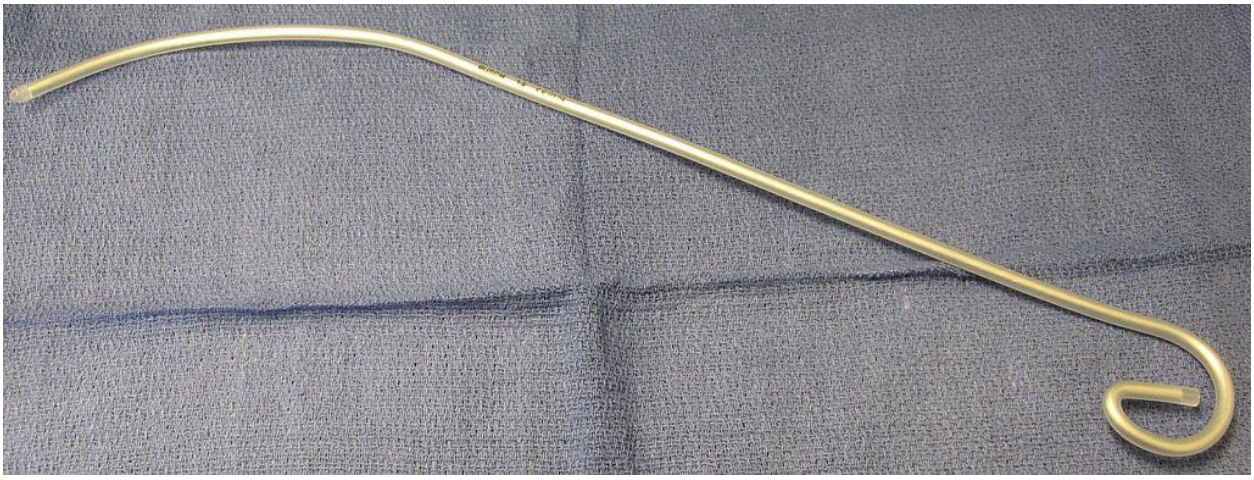

Figure 5. An image of an intubating stylet. Most stylets are made from aluminum coated in a flexible plastic sheath. The stylet is used to provide shape and structure to the ET tube making it easier to guide down the throat.

"Tracheal tube stylet" by DiverDave. Licensed under CC BY 3.0 via Wikimedia Commons, used with permission 2015.

https://commons.wikimedia.org/wiki/File:Tracheal_tube_stylet.JPG#/media/File:Tracheal_tube_stylet.JPG

To pass the ET tube into the throat doctors and EMT's use a tool called laryngoscope. This device consists of two parts: a handle and a set of interchangeable laryngoscope blades. This device serves several functions. Primarily, it is used to guide the ET tube down the throat and into the trachea. It is also used to manipulate the epiglottis and tongue to facilitate visualization of the vocal cords. Most laryngoscopes have a light, which helps illuminate the mouth and throat. The blades come in two styles and several different sizes. These two styles are the Macintosh blade and Miller blade. The difference in shape changes how the blade manipulates the glottic aperture. Macintosh blades are used to pull the epiglottis forward and away from the vocal cords whereas Miller blades are used to apply pressure to the supraglottic fold bringing the glottic aperture into view. Usage of one blade over another is often dictated by operator preference, though patient anatomy sometimes dictates which blade is used. Different blade sizes allow the device to be used in a wide variety of patients. A laryngoscope along with the two blade types can be seen in Figure 6[1].

Figure 6. A laryngoscope with its two different blade types. The laryngoscope is used to manipulate the tongue and glottis aperture to allow for visualization of the vocal cords as well as guide the ET tube down the throat.

"Macintosh Blades" by Sasata (talk) - I (Sasata (talk)) created this work entirely by myself.. Licensed under CC BY 3.0 via Wikipedia, used with permission 2015
https://en.wikipedia.org/wiki/File:Macintosh_Blades.jpg#/media/File:Macintosh_Blades.jpg
"Laryngoscopes-Miller blades" by User:DiverDave. Licensed under CC BY 3.0 via Wikimedia Commons, 2015 https://commons.wikimedia.org/wiki/File:Laryngoscopes-Miller_blades.JPG#/media/File:Laryngoscopes-Miller_blades.JPG

Intubation Procedure

There are several types of intubation that are performed on a regular basis, but for the purpose of this design, only oral rapid sequence intubation (RSI) is being considered as it is the procedure most commonly used in emergency settings. RSI is used when there is a risk of the patient aspirating gastric contents, which prevents the use of bag and mask ventilation. The procedure uses a powerful induction agent and a neuromuscular blockade to render the patient unconscious, relax the muscle of the throat, and most importantly suppress the gag reflex in the patient. Because the patient is essentially paralyzed during the procedure and unable to breathe on their own, esophageal intubation becomes a major concern[1].

The procedure starts with the physician or EMT preparing the tools needed for intubation. Next, the patient is pre-oxygenated with 100% oxygen for 3 to 5 minutes. This ensures that there is enough residual oxygen in the blood and lungs to allow for several minutes of apnea before desaturation of the hemoglobin. Next, the patient is given several drugs to help mitigate some of the negative effects of intubation and the paralytic agents used to facilitate RSI. Next, the induction and paralytic agents are administered, rendering the patient unconscious and paralyzed. Next the intubation is performed. First, the laryngoscope is inserted into the mouth toward the throat and glottic aperture. The insertion happens at an angle that allows the tongue to be swept out of the way by the blade. The laryngoscope is lifted pulling the tongue forward revealing the glottic aperture. However, it should not be levered, as this can cause damage to the patient's teeth and jaw. Once the glottic aperture is visualized, the tube should be advanced down the laryngoscope guide through the cords and into the trachea. Next, the balloon cuff is inflated to secure the tube in position. Tube placement is then confirmed using several of the tube confirmation methods to be discussed in the next section. After the tube is placed and confirmed, the ET tube is secured to prevent accidental removal[1].

Tube Placement and Confirmation

The confirmation of endotracheal tube placement is arguably the most important step in the procedure. Because the patient is paralyzed, it is vital that the tube be in the right position,

otherwise they will not receive adequate oxygen. There are many tools and methods available to doctors and EMTs to assess tube placement and each has their own advantages and disadvantages. It should be noted that no one method provides a definite answer about tube position, meaning multiple independent verifications are needed to establish correct tube placement [1].

Direct Visualization

One simple method of tube placement is visualization of tube passage through the vocal cords. This is often the first step in confirming that the procedure has been performed correctly. It involves watching the end of the endotracheal tube pass through the vocal cords and into the trachea during the intubation procedure. While an integral part of intubation, it alone is not sufficient to confirm tube placement [1]. Because of the complex geometry of the throat and the inherent variability in structure from person to person, this observation can be very subjective. The issue is further compounded when an airway is swollen, injured, or obstructed, making the relevant anatomy difficult to visualize. In some cases, this difficulty can be an indicator that the intubation procedure should not be performed and an alternative method should be attempted. As this method can be subjective, it is always necessary to use another verification method, such as end tidal CO_2 to further confirm tube placement.

End Tidal CO_2

End tidal CO_2 is currently the gold standard for confirming proper tube placement. End tidal CO_2 monitors the expired CO_2 of a patient to ensure that they are being properly ventilated. By monitoring the exhaled CO_2 concentration, it becomes possible to determine if the patient is being correctly ventilated. This method shows high sensitivity, specificity, and is also fairly easy to implement[6].

There are two main methods of measuring CO_2 levels: waveform capnography, and disposable end tidal CO2 detectors. During waveform capnography, CO_2 levels are monitored and displayed as a waveform, plotting concentration versus time. During the exhalation phase of ventilation there is a sharp increase in CO_2 concentration followed by a sharp decrease in concentration at the start of inhalation phase. If properly ventilated, this waveform should appear as a square wave. Improper intubation will either produce no wave form or one that is attenuated[7].

There are also disposable end tidal CO_2 detectors that use a paper discs with CO_2 sensitive ink to detect the presence of expired CO_2. When attached to the ET tube the paper disk will change colors in a few breaths if the patient is properly ventilated. If it does not change quickly, then there is a good indication that the patient has not been intubated correctly[7].

Esophageal Intubation Detector

Another device for detecting esophageal intubation is the aptly named esophageal intubation detector or EID. This device works on the principle that the esophagus is much softer than the trachea. The trachea is held open by rings of cartilage but the esophagus is made of soft muscle. An EID consists of a squeeze bulb and an adapter for the ET tube. The squeeze bulb is emptied of air and then attached to the end of the ET tube. The bulb is then released and allowed to fill with air. If the ET tube is in the esophagus, the suction from the bulb will cause the esophagus to collapse around the end of the tube and prevent the bulb from fully inflating, or slow down its rate of inflation. If the tube is placed in the trachea the bulb should fill quickly[1]. This device has the advantage that it works well in cardiac arrest patients where end tidal CO_2 cannot function. While this device has been proven to be as accurate as end tidal CO_2 in detecting Esophageal intubation[8] it is still subject to some level of misinterpretation. Since the primary indicator is bulb fill-speed it is up to the EMT to judge whether the bulb filled fast enough to indicate tracheal intubation.

Undetected Esophageal Intubation

If these detection methods fail or are misapplied there is a serious risk of undetected esophageal intubation. Undetected esophageal intubation is one of the most serious complications that can occur during the intubation procedure. It is important to distinguish this from esophageal intubation as it affects the scope of research being performed. Esophageal intubation in and of itself is not particularly dangerous. In fact, it occurs fairly often with EMTs and doctors often missing their first attempt but placing the tube successfully on their second try[1]. When an endotracheal tube is placed in the esophagus, the EMT simply has to remove the tube and attempt another intubation, after a certain number of failed attempts (usually three) an alternate method of establishing an airway should be attempted[1]. Primary issues caused by repeated esophageal intubation include an irritated airway and a chance for perforation of wall of the pharynx. While

these are undesirable and should be avoided, neither of these two complications are immediately life threating.

However, undetected esophageal intubation is extremely dangerous and must be avoided at all cost. As the name suggests undetected esophageal intubation happens when an endotracheal tube is placed in the esophagus and incorrectly identified as being placed in the trachea. This leads to the erroneous assumption that a viable airway has been established when it has not. A number of complications occur with undetected esophageal intubation. First is the fact that the patient receives no oxygen to the lungs as any air entering the body is going into the stomach. The patient quickly deoxygenates and hypoxia begins. Since the patient is paralyzed, they cannot breathe on their own, even if they had a semi-viable airway before the procedure. Within minutes, organ failure and brain death occur. Even if the error is detected later in the procedure, there is a strong likelihood that the patient will have lasting brain damage [2].

The next major complication comes from the fact that the stomach is being ventilated instead of the esophagus. The extra air in the stomach can cause the patient to passively regurgitate gastric contents. If aspirated, these contents will further complicates the airway. A simple airway can quickly turn into a failed airway mandating the need for surgical airway techniques such as a crycothrotomy. This aspiration also opens up the patient to the risk of severe respiratory infections, which can prove fatal.

While establishing a list of causes for undetected esophageal intubation is difficult due to the varied nature of the emergency medical field, a few causes are often seen. The first commonly identified cause is inexperience. While the intubation procedure sounds conceptually simple, it is in fact very difficult, requiring both strength and manual dexterity. Applying too much force will injure the patient's teeth and jaw. Applying too little force can cause the operator to lose sight of the vocal cords and other target anatomy. Without proper training, it is easy to misidentify anatomy or lose sight of the target anatomy in the throat. This leads to esophageal intubations or cases where the operator is unsure of tube placement. Again, without proper training, it is also difficult to realize when the procedure has been performed incorrectly [3].

The next and, least excusable cause is over-confidence. Many senior doctors and EMTs become so proficient at intubation that they become over confidant in their skills. It has been reported that in many cases of UEI that the doctor believed that they had intubated a patient

correctly when they had not. This over-confidence also leads to doctors failing to believe the output of their machines and other detection methods [4].

Automatic Intubation Detection Devices

In order to address the shortcomings with current esophageal intubation detection methods, several automatic assessment methods have been proposed. Automating the assessment of tube position reduces this risk for operator error and misinterpretation of data. This section will provide a brief overview of these automated methods to introduce some of the work that has already been done in this field.

One such device looked at instrumenting an EID to measure the pressure change in the system. The design proposed that by measuring the pressure in the bulb or syringe of the EID it would be possible to determine whether the ET tube was in the esophagus or the trachea. While the principle of operation for this device is sound, no peer reviewed articles could be found assessing its performance. However the patent is available for public review[9].

Another automatic detection solution suggested measuring the change in acoustic properties of the endotracheal tube caused by esophageal intubation. Because the esophagus is compliant, it was theorized that the esophageal wall would occlude the end of the endotracheal tube more than the ridged trachea. This occlusion should cause a change in the resonance frequency of the tube. Sending sound waves through the tube, it should be possible to measure this change in resonance and evaluate whether the tube has been placed correctly or not. The major downside to this method is that it requires calibration of the device before every procedure. Again, while the patent is available, no peer reviewed articles were found to verify the devices performance[10].

A final method for automatic endotracheal tube placement used video laryngoscopy and computer vision. The proposed device used a video fiber optic scope to guide the ET tube down the throat. Images from the end of the video stylet were processed using a computer vision algorithm. This algorithm used a feature detector and a machine-learning algorithm to classify different anatomical landmarks in the throat and larynx. If certain anatomical landmark such as the vocal cords or tracheal rings were detected, then the device would indicate a correct intubation. The research paper on the device showed that it had a high specificity and accuracy for assessing intubation methods. While the results were promising, it did have some issues. During the paper, the device was only tested on clean uninjured airways. Due to its reliance on images, there is some

concern as to how well it would function in situations with airway damage or obstructions. The other issue was that the computing power required was rather high. With current computing technology, the devices computer would be either too big or too expensive to implement[11].

GMR Principles

Before discussing the design of the automatic detection device in this thesis, it is important to understand some of the theory behind its sensor element. This device uses a giant magnetoresistance (GMR) sensor to measure the distance between a magnetic probe on the end of the ET tube and a sensor at the surface of the neck. A GMR sensor changes its resistance in the presence of an applied magnetic field; the higher the field strength, the lower the resistance in the GMR element. This change in resistance, can range from anywhere between 4% and 20% depending on materials used to make the sensor[12].

GMR sensors work by changing the mean free path of electrons inside a material. In very thin layers of material, an electron tends to scatter off the boundary of the layer instead of traveling its entire mean free path. This results in an increase in resistance in the material when it is only a few molecules thick. GMR sensors work by changing the mean free path of these electrons through the application of a magnetic field[12].

A thin layer of conductive material is sandwiched between two magnetic sheets of material. These two magnetic sheets are anti-ferromagneticly coupled, giving them magnetic fields that are opposite of one another. Electrons moving through these magnetic materials adopt spin characteristics, with spin up electrons in the upper layer and spin down electrons in the bottom layer. Because of their spin, these electrons tend to scatter off the opposite layer, shortening their mean free path (Figure 7).

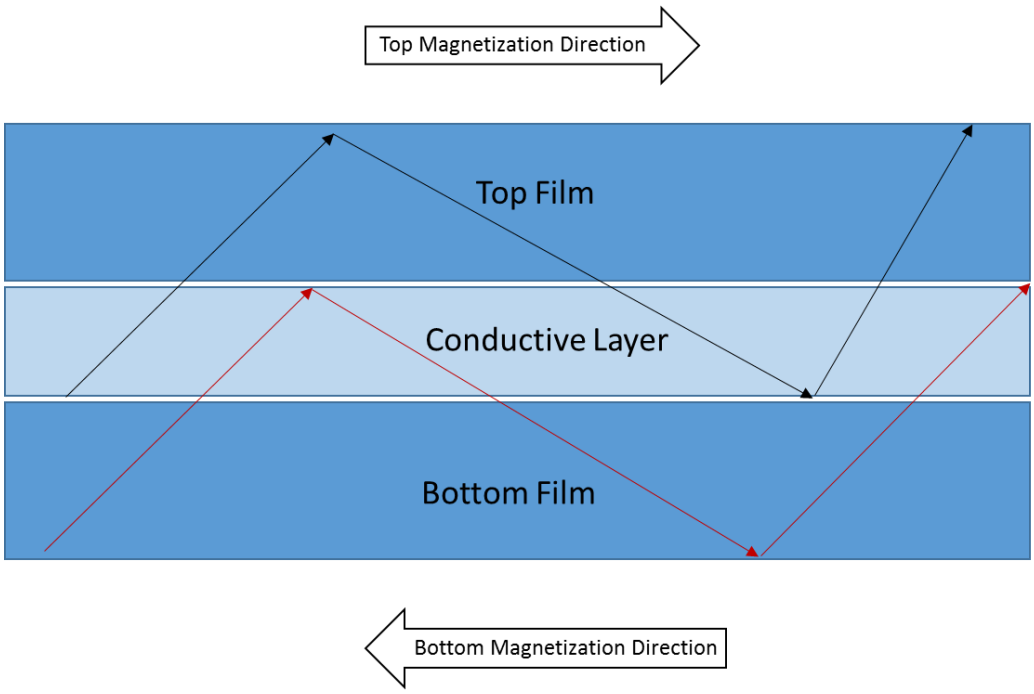

Figure 7. A diagram of electron scattering in a GMR element. The top and bottom layers of the GMR element are anti anti-ferromagneticly coupled. Electrons scatter off of the oppositely magnetize layers shortening there mean free path and increasing the resistance of the element [12]

When a sufficiently strong magnetic field is applied, it can reverse the magnetization direction of one of the layers, as seen in Figure 8. This in turn changes the spin characteristic of electrons flowing through that layer, giving them all the same spin. Electrons no longer scatter at the layer boundaries and their mean free paths increase. This causes the large resistance drop normally seen in GMR sensors[12].

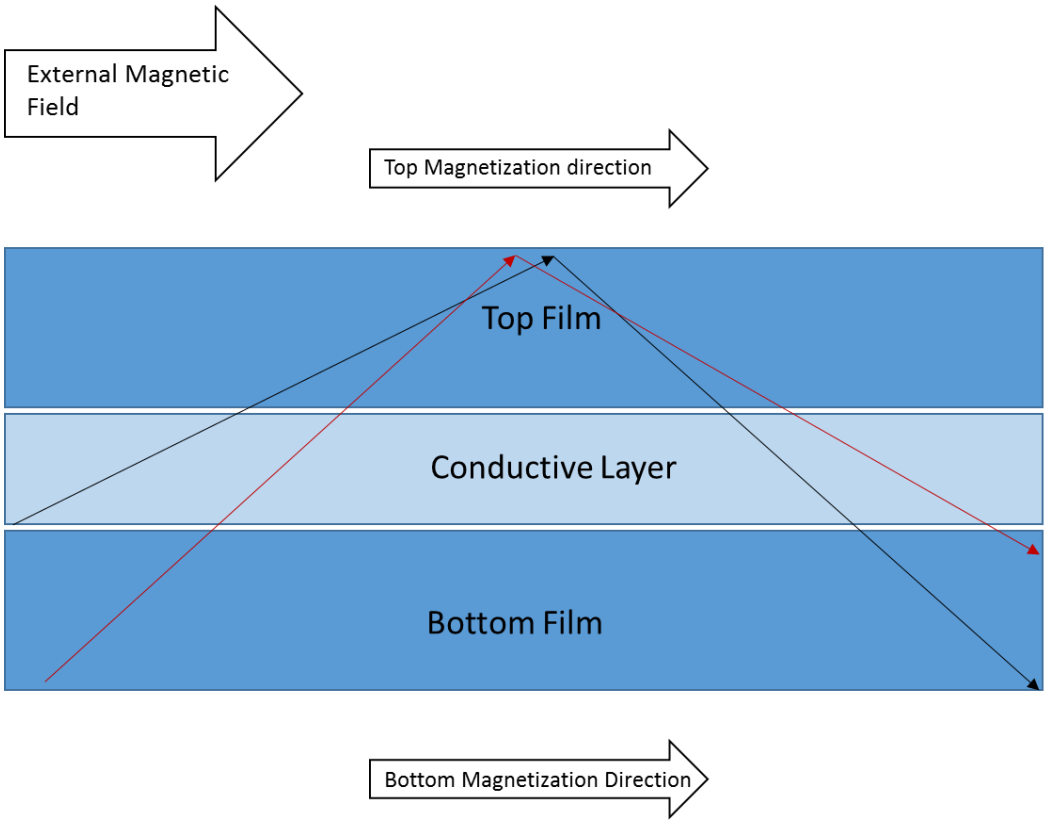

Figure 8. In the presence of an external magnetic field, all of the GMR layers have the same magnetic polarization. Electrons in the top and bottom layers have the same spin, so they stop scattering at the layer boundaries. This causes the mean free paths to increase and the resistance of the element to drop[12].

Chapter 3. Method

This chapter will look at the design decisions and methods used to develop the device. First, the chapter will provide an overview of the primary parameter used to detect esophageal intubation and tracheal intubation as well as why this value is a valid indicator of these two intubation states. Next, this chapter will describe and validate the key assumptions made during the design of the device. Then, this chapter will examine the conceptual design of the sensor as well as some of the driving equations behind the detection method. Finally, the chapter will provide an overview of the detailed sensor design, describing parts selection and specifications along with diagrams and the device layout.

Proposed Method for Automatically Assessing Tube Position.

In order to detect the difference between an esophageal intubation and a tracheal intubation, this device will measure the distance from the surface of the neck to an ET tube inside the neck. In normal human anatomy, the trachea sits in the anterior part of the neck directly below the larynx. The esophagus, however, is located near the center of the neck, behind the trachea and surrounded by muscle and soft tissue. This means that an endotracheal tube placed correctly into the trachea should be much closer to the surface of the neck then a tube incorrectly placed in the esophagus. By measuring the distance between the endotracheal tube and the surface of the neck, it should be possible to assess endotracheal tube placement directly. This satisfies the goal of direct observation since it assesses tube position independent of the physiological state of the patient.

At its simplest form, a distance measurement below a critical value would indicate tracheal intubation and a distance above that critical value would indicate esophageal intubation. Determination of a critical value that works in most average adult patients is a major design consideration of this project. This value needs to be high enough that it allows the device to function in a wide variety of patients, but low enough to prevent false positive indications of tracheal intubation.

To measure this distance, this project will use a giant magnetoresistance sensor and a magnetized stylet. The magnetized stylet produces a static magnetic field that is detected by the GMR sensor. Since magnetic field strength is a function of distance, it is possible to relate the

output of a GMR sensor on the surface of the neck to the depth of the ET tube and intubating stylet in a person's upper airway. The signal from the magnetized stylet is attenuated with distance, but magnetic fields are not strongly affected by human tissue[13]. This means that the variability in strength of the magnetic field is primarily effected by distance. This makes magnetism a strong candidate for automated evaluation as the only effect on the magnitude of the output is the distance from the sensor. A diagram of this detection method can be seen below in Figure 9.

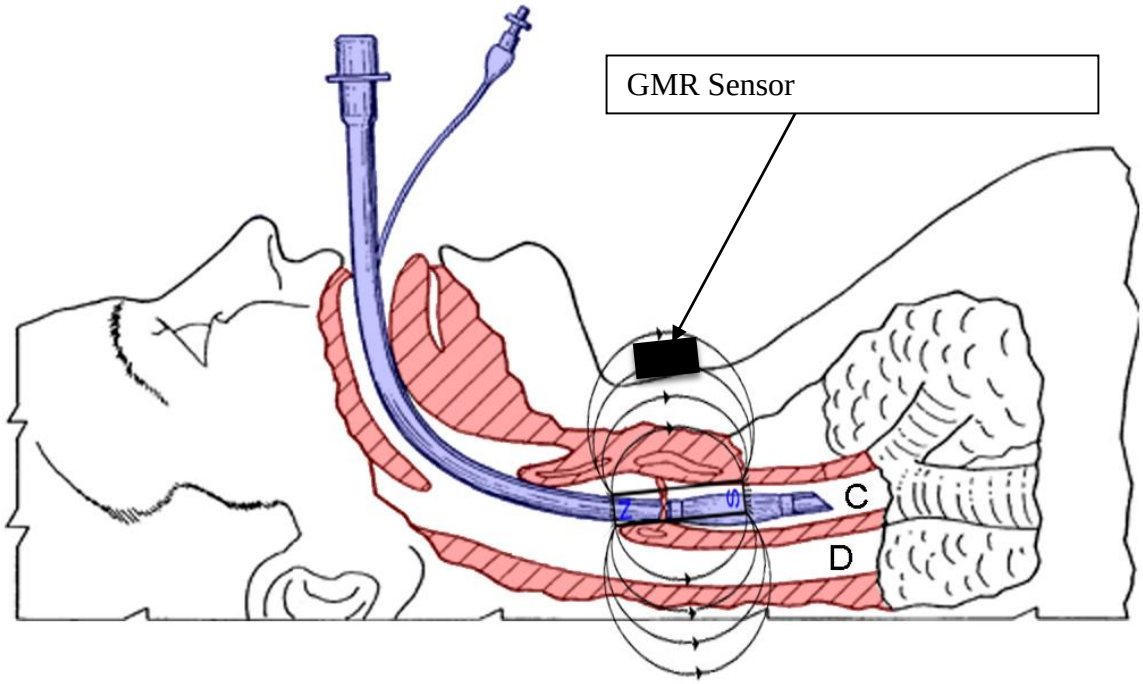

Figure 9. A diagram of the proposed detection method. A giant magnetoresistance sensor on the surface of the neck will be used to measure the depth of a magnetized intubating stylet from the surface of the neck. Since the trachea (C) sits above the esophagus (D), an ET tube in the trachea will be much closer to the surface of the neck then an ET tube in the esophagus. Determining the proper depth at which a tube can safely be considered in the trachea is a major component of the design process for this device.

"Endotracheal tube colored" by PhilippN - Modification of Licensed under Public Domain via Wikimedia Commons, public domain, 2015
http://commons.wikimedia.org/wiki/Image:Endotracheal_tube_inserted.png.

By connecting the GMR sensor to a DAQ or microcontroller, the assessment of tube placement can be automated. With the proper value for critical depth, the computer or microcontroller only needs to check if the stylet is above or below that critical value. This means that the user only needs to interpret a binary indicator from the system instead of having to make a judgment based on an analog signal.

The principle of measuring tube depth inside the neck has been demonstrated successfully before in a device called a lighted stylet. A plastic stylet with a bright light on the end is used to guide the intubation tube into the trachea like a regular intubating stylet. Tube depth and position are monitored by observing the trans-illumination of the tissue in the neck. A tube in the trachea will appear as a bright dense dot at the surface of the neck while a tube in the esophagus will appear as dull diffuse light at the sides of the neck. While this method has been shown to be very effective, it still requires proper interpretation by a skilled operator to be used effectively [14].

Assumptions

Several key assumptions must be made before the magnetic assessment method described in the previous section can be implemented. The first and most important relates to the magnetic permeability of human tissue. Magnetic permeability refers to the effect a material has on the propagation of magnetic fields passing through it. Materials with permeability less than that of free space attenuate magnetic fields while materials with a permeability greater then free space accept magnetic fields. In the case of human tissue, the magnetic permeability is close to that of the permeability of free space. This means that human tissue has a weak effect on the propagation of magnetic fields. While not exactly the permeability of free space, the permeability of most human tissues are so close that they can all effectively be considered μ_0. Figure 10 shows several common human tissues and their magnetic permeability [13]. This graph was taken from a study on MRI compatibility of different tissues. While the small differences in permeability are important for MRI research, they are well below the noise floor of any sensor that will be used in the project.

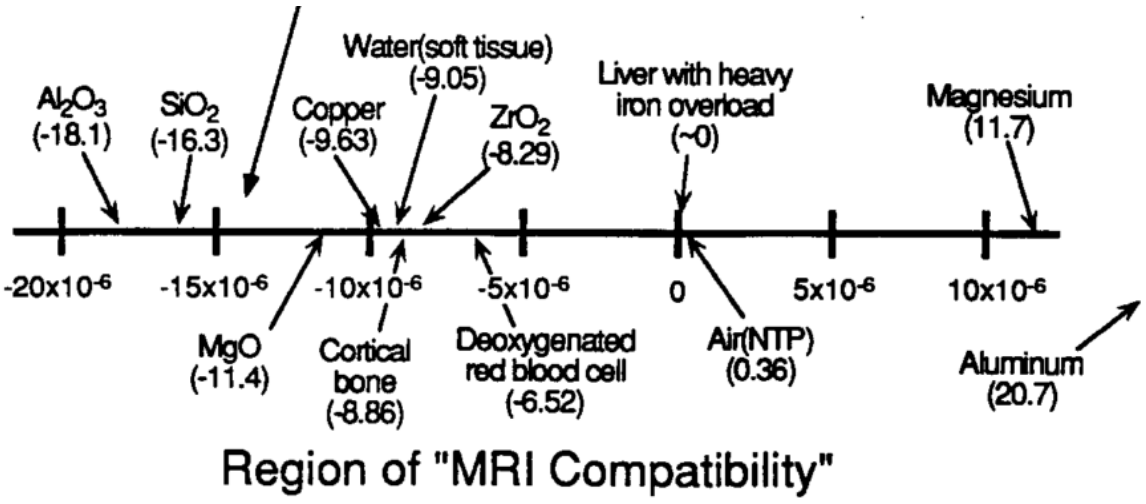

Figure 10. A chart with MRI compatibility and magnetic susceptibility of several common human tissue types [13]. *Most human tissues have a magnetic permeability close to that of vacuum. This means that the composition of tissue in the neck will not have a significant effect on the sensor's operation.*

J. F. Schenck, "The role of magnetic susceptibility in magnetic resonance imaging: MRI magnetic compatibility of the first and second kinds.," Med. Phys., vol. 23, pp. 815–850, 1996.

The next assumption has to do with the effect that the magnetic field will have on several of the devices used during the intubation procedure. First is that the laryngoscope blade being used in the procedure is non-magnetic. Most blades are advertised as being made of "surgical steel." While this can mean they are made of 316, 402, or 440 steel, it will be assumed that the blades used with this device are made from 316 steel. This steel grade is nonmagnetic due to its crystal structure, meaning that it will be less likely to interact with the emitter at the tip of the stylet. The laryngoscope blades used in testing exhibit no ferromagnetic properties. The handle and batteries of the laryngoscope are assumed to be far enough away from the stylet to have little to no effect on the sensor. It is also assumed that a typical adult male patient does not have any metal or magnetic sensitive implants on or near their body that would interact with the sensor or probe. With these assumptions in place, it becomes possible to derive a critical distance inside the neck that depends only on the position of the tube inside the neck.

Derivation of Critical Depth in Neck and Statistical Assessment of Neck Anatomy

The most important part of this detection method is determining the critical distance from the surface of the neck that indicates esophageal intubation. Distance measurements above this value indicate esophageal intubation while measurements below indicate tracheal intubation. If

this critical distance is too small, the device will fail to recognize proper intubation and if it is too large, it could potentially indicate that device is in the trachea when it is actually in the esophagus. As stated earlier, case two should be avoided at all costs, as it can lead to cases of undetected esophageal intubation. In order to avoid this, it is necessary to use conservative estimations when deriving this distance.

Estimating this value requires knowledge of the dimensions of a normal human trachea and the soft tissue surrounding it. The parameters needed to determine this critical value are tracheal diameter, tracheal wall thickness, esophageal wall thickness, and pre-tracheal soft tissue thickness. Ideally, these values would be constant, making the estimation a sum of the different thicknesses. Unfortunately, the human body is highly variable which means that instead of constants it is only possible to obtain mean distances with upper and lower bounds on thickness. Figure 11 shows a neck cross section along with several of these key distances that need to be estimated.

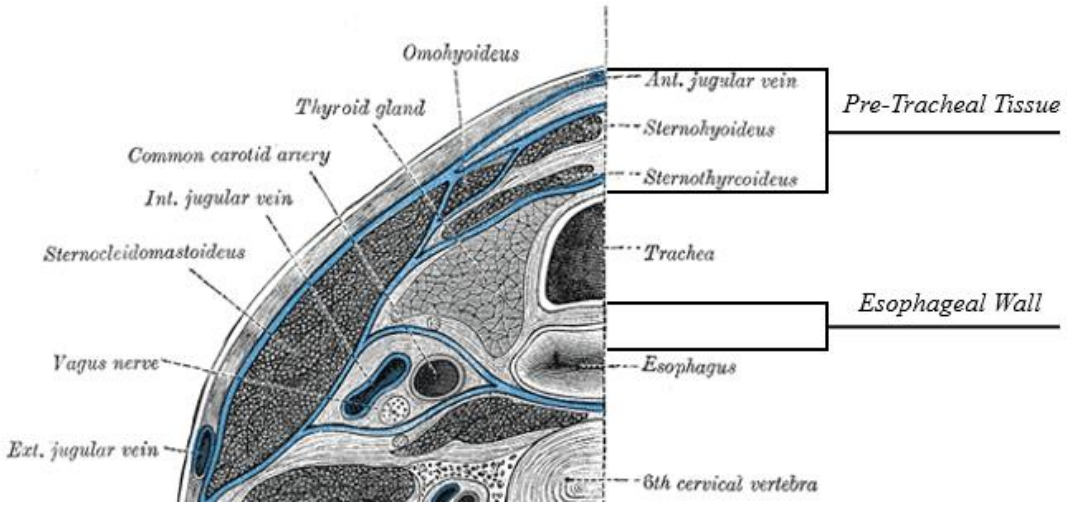

Figure 11. A cross section of the human neck. The pre-tracheal tissue thickness is the sum of all of the tissues between the surface of the neck and the trachea wall. The esophageal wall thickness is taken to be the distance between the back wall of the trachea and the front wall of the esophagus.

"Gray384" by Henry Vandyke Carter - Henry Gray (1918) Anatomy of the Human Body (See "Book" section below)Bartleby.com: Gray's Anatomy, Plate 384. Licensed under Public Domain via Wikimedia Commons, public domain, 2015
https://commons.wikimedia.org/wiki/File:Gray384.png#/media/File:Gray384.png

In order to derive a set point, two separate sums of anatomical distance will be calculated and then compared. The first is the sum of the pre-tracheal tissue thickness (PTT), tracheal wall thickness (TWT), and the tracheal radius (TR). Also included in this sum is an estimate of the

uncertainty of the position of the ET tube inside the trachea (Pu). This sum gives an estimate of the distance from the surface of the neck to the tip of the ET tube inside the trachea along with the uncertainty in that position.

The next important sum of measurements estimates the distance and uncertainty from the surface of the neck to the front wall of the esophagus. This sum includes the pre-tracheal tissue thickness (PTT), the tracheal wall thickness (TWT), the tracheal diameter (TD), and the esophageal wall thickness (EW). This will give the closest expected distance the ET tube can be and still be considered in the esophagus. Estimates of each of the individual distances that make up these sums will be derived in the next section.

Depth Estimations

The first distance to be estimated is the tracheal diameter (TD). Since the sensor will be viewing the trachea from front to back, this estimate will refer to the sagittal diameter of the trachea. This value was reported in a paper on the normal dimensions of a human trachea. In this paper, the group measured tracheal diameters of multiple patients at 2 cm above the aortic arch using x ray. In this paper, they indicate that the average adult male trachea is 20.25±2.25 mm. This measurement came from a survey for patients from multiple age groups and demonstrated that there was little change in the mean tracheal diameter with ages above 20 [15].

The next two anatomical measurements of importance are the tracheal wall thickness and the esophageal wall thickness. An estimation of tracheal wall thickness is necessary as it adds to the overall thickness of the neck above the trachea. This value was found to be 4.7±.89 mm from a paper on the relationship between certain cancers and tracheal wall thickening [16]. In this paper, the authors took multiple transverse slices of human trachea and measured the thickness of the tracheal cartilage with an optical micrometer.

The esophageal wall thickness determines the amount of space between the tracheal and esophageal lumen. The average esophageal wall thickness was found to be 5.26±.93 mm [17] and comes from a paper on the assessment of normal esophageal dimensions from CT images. In this paper, they measured the dilated and contracted esophageal wall thickness during swallowing. The dilated wall thickness was used as the esophageal muscles are only contracted during swallowing.

The next neck thickness of importance is the pre-tracheal tissue thickness. This thickness is the most important but also the hardest to accurately define. Pre-tracheal tissue is made mostly

of subcutaneous fat meaning that it is highly variable with patient weight. These values were estimated from a paper on the relationship between pre-tracheal tissue thickness and several common methods for assessing patient weight. In this paper the researchers found a linear relationship ($R^2 = 82.4$) between waist circumference and pre-tracheal tissue thickness [18]. The linear regression of this data is shown in Equation 1, where PTT is the pre-tracheal tissue thickness in centimeters and the WC is the waist circumference in centimeters.

$$\boldsymbol{PTT = .02 * WC - .91} \quad \textbf{(1)}$$

The information from this paper was combined with data on waist circumference from a CDC paper on average anthropometric values for the United States. This combined data set was then used estimate the mean and uncertainty of pre-tracheal tissue thickness in the adult male population. Mean waist circumferences (100.9cm) along with waist diameters of the 5th (77.8cm) and 95th (128.2cm) percentiles of the population were plugged into the regression model from the pre-tracheal tissue thickness paper to get an estimated pre-tracheal tissue thickness of 11.08±5.02mm. It should be noted that this estimate only captures the mean of the population and not the variation at the 5th and 95th percentile. Better data on pre-tracheal tissue thickness is needed to address this shortcoming in this part of the model.

The last distance measurement is the uncertainty in the position of the endotracheal tube inside the trachea. Since the ET tube's diameter is smaller than the tracheal diameter there is some degree of variability as to how far from the center of the trachea the tube tip can be. This value can be estimated by subtracting twice the wall thickness of the ET tube from the diameter of the trachea and then plugging this value into calculation of variance for a continuous random distribution, as seen in the Equation 2 and illustrated in Figure 12 below.

$$\boldsymbol{Pu = \sqrt{\frac{(TD \pm 2\sigma - 2 * T_{wall})^2}{12}} * 2} \quad \textbf{(2)}$$

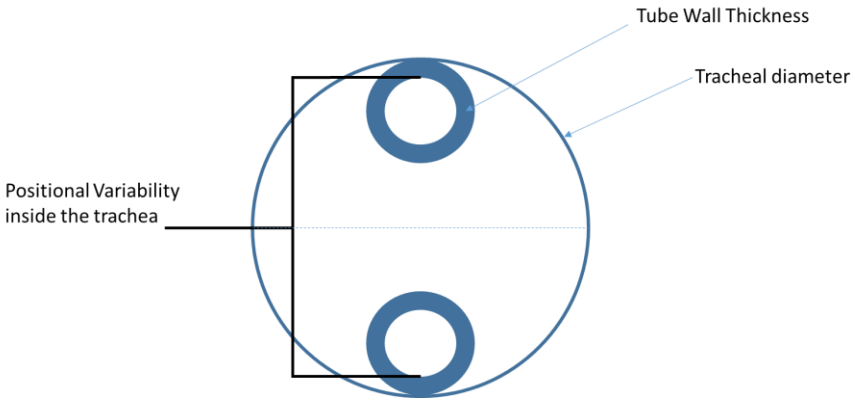

Figure 12. A diagram showing the positional variability of an ET tube inside the trachea. It is assumed that the tube has equal probability of being in any position inside the trachea minus the wall thickness of the ET tube.

Derivation of Critical Depth

Using the distance values and uncertainties derived above, it now becomes possible to estimate the distances from the surface of the neck to the center of the trachea and the front wall of the esophagus. This will provide predicted tracheal and esophageal distances of the ET tube and allow for the calculation of the critical distance.

Summing the pre-tracheal tissue thickness, the tracheal wall thickness, tracheal radius, and the positional uncertainty of the ET tube, it was found that for an average adult male, the distance to the center of the trachea is 25.905 ± 10.99mm (Equation 3). Summing the pre-tracheal tissue thickness, the tracheal wall thickness tracheal diameter and esophageal wall thickness it was found that the distance to the front wall of the esophagus 41.21±5.981mm (Equation 4).

$$(\boldsymbol{PTT} \pm \boldsymbol{2\sigma}) + (\boldsymbol{TWT} \pm \boldsymbol{2\sigma}) + .\boldsymbol{5}(\boldsymbol{TD} \pm \boldsymbol{2\sigma}) + (\boldsymbol{0} \pm \boldsymbol{PV}) \quad \textbf{(3.a)}$$

$$(\boldsymbol{11.08 \pm 5.02}) + (\boldsymbol{4.7 \pm .89}) + (\boldsymbol{10.125 \pm 1.125}) + (\boldsymbol{0 \pm 9.675}) = \boldsymbol{25.905 \pm 10.99mm} \quad \textbf{(3.b)}$$

$$(\boldsymbol{PTT} \pm \boldsymbol{2\sigma}) + (\boldsymbol{TWT} \pm \boldsymbol{2\sigma}) + (\boldsymbol{TD} \pm \boldsymbol{2\sigma}) + (\boldsymbol{EWT} \pm \boldsymbol{2\sigma}) \quad \textbf{(4.a)}$$

$$(\boldsymbol{11.08 \pm 5.02}) + (\boldsymbol{4.7 \pm .89}) + (\boldsymbol{20.25 \pm 2.25}) + (\boldsymbol{5.26 \pm .89}) = \boldsymbol{41.29 \pm 5.643mm} \quad \textbf{(4.b)}$$

It should be noted that these two values overlap, with the closest esophageal distance at 35.647 mm and the furthest tracheal distance at 37.695mm. Because of this overlap, there is no set point that can cover the entire population. However, as discussed earlier, the failure mode that must be avoided is false positive indication of tracheal intubation. By allowing for a higher false negative rate in the patients with high PTTs, it becomes possible to develop a set point that can be safely used with the majority of the population. This set point will be set at the mean esophageal distance minus three standard deviations from that mean. Three sigma is chosen as it ensures that 99.7% of the population will have an esophageal distance greater than the selected value. This gives a critical point value of 32.8255mm. It was found that this value would indicate true tracheal intubation in 89.7% of the population, with false negatives occurring in the top 11% of the population for pre-tracheal tissue thickness. While higher than desired, false negative results are much less dangerous than false positive results. These estimates are undoubtedly optimistic and do not factor in sensor uncertainty, meaning rigorous testing on a wide population will be needed to fully validate safety of this set point.

Conceptual Sensor Design

With a proper set point in place, it now becomes possible to design the distance sensor that will assess tube position inside the throat. As stated earlier, the device is composed of two parts: a ferromagnetic emitter embedded in the stylet used to guide the ET tube and a GMR sensor placed on the surface of the neck. The magnetic stylet consists of a standard intubating stylet made of plastic or rubber-coated wire with a magnet attached or embedded on the tip. The magnet is a cylindrical bar magnet with known magnetization and material compositions and has the same diameter as the intubating stylet.

The GMR sensor is a standard single pole sensor whose output changes with the application of a static magnetic field. The sensor is placed on the surface of the patient's neck just above the suprasternal notch. The output from the GMR sensor is then interpreted by a DAQ or microcontroller. The microcontroller or computer has an interface that indicates when the magnetic emitter is closer than previously derived critical threshold alerting the user to proper tracheal intubation or further away indicating improper intubation.

During the procedure, the magnetic stylet and ET tube are guided into the patient's airway according to standard intubation procedure. As the magnetic emitter passes in front of the GMR sensor, the strength of the magnetic field around the sensor changes. If the field strength is higher than the field strength at the critical distance of 32.8255mm, the device will indicate tracheal intubation while if the field strength is lower than the critical value it will indicate improper intubation. Figure 13 shows the proposed layout of the emitter inside the neck with the ET tube during an intubation procedure.

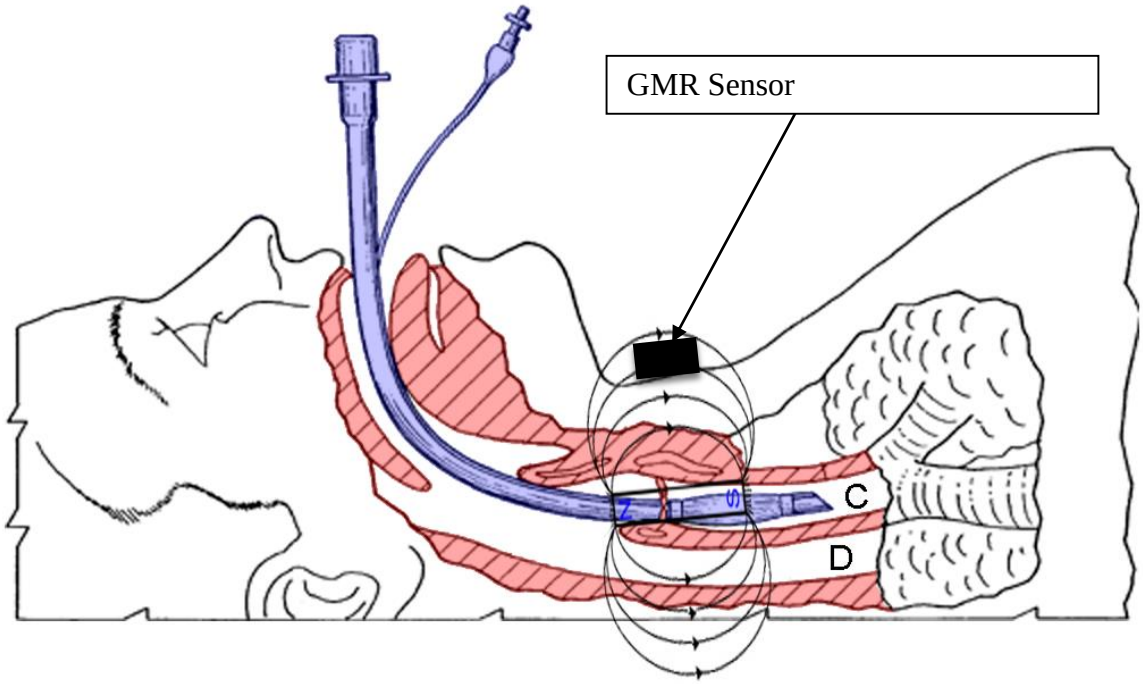

Figure 13. A diagram of the magnetic field of the emitter inside the neck. An intubating stylet with magnetic tip placed inside an ET tube. During the intubation procedure, the GMR sensor monitors the strength of the magnetic field inside the neck. If the field strength exceeds a certain value it indicates, a tracheal intubation while a low value indicates esophageal intubation.

Modification of "Endotracheal tube colored" by PhilippN - Licensed under Public Domain via Wikimedia Commons, 201, public domain, 2015
http://commons.wikimedia.org/wiki/Image:Endotracheal_tube_inserted.png.

Detailed Design

With proper estimate for the critical depth, it becomes possible to select the sensors and components needed to build a sensor for measuring this distance. This section will outline this selection process as well as describe the design of the entire system in detail.

Sensor Selection

The first step in this detailed design was selecting a suitable GMR sensor. This sensor needed to be easy to use and implement, as well as be sensitive to a wide range of magnetic field strengths. One such sensor series that satisfied this was the NVE AA GMR sensor series. These sensors came in a wide variety of sensitivities from 0.1 oersteds to 100 oersteds. For the initial testing a sensor with a linear range from 10 to 70 oersteds was chosen. This was the highest range sensor, and while not as sensitive to small changes in oersteds values, it would provide a wide range of field strengths that could be tested.

This sensor has a linear range from 10 to 70 oersteds with a saturation value of 100 oersteds. The sensor can still read changes in magnetic fields below 10 oersteds and above 70 oersteds but the relation between resistance and field strength will be non-linear and is not documented in the spec sheet. However, this is not seen as a problem as the critical point lies within the linear range of the sensor. The sensitivity of the sensor is nominally .5 mv/V/Oersteds, meaning that a change of one oersteds produces a 0.5 change in output times the bridge operating voltage. The sensor consists of a single GMR sensor element in a bridge configuration. When a magnetic field is applied to the GMR sensor, the change in resistance can be measured as a change in voltage across the bridge. The bridge resistance is nominally 5k with a zero magnetic field. The sensor experiences some hysteresis of 4% at maximum output. This is due to some residual magnetization in the GMR element after the application of a strong magnetic field. The sensor itself is very tolerant to high magnetic fields and under the expected operating conditions, damage to the sensor from contact with the magnet is not expected. Figure 14 shows the sensor mounted to its breakout board with its four leads attache.

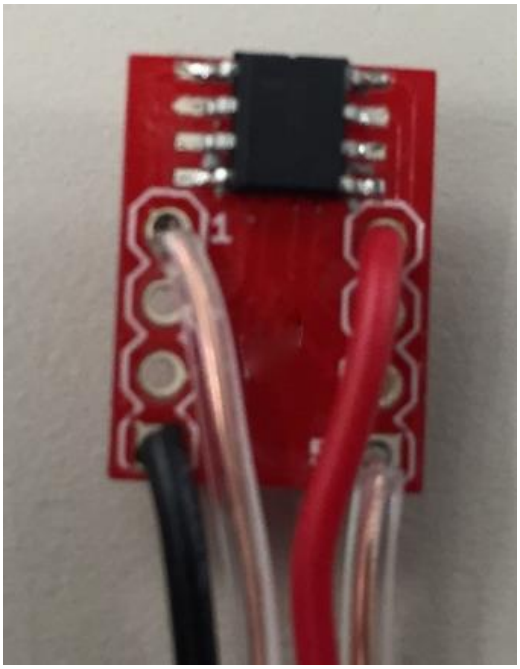

Figure 14. An image of a NVE GMR sensor mounted to its SOIC-8 breakout board. The red and black wires are for power and ground while the two clear wires are for monitoring the voltage across the bridge.

The final magnet selected for the project was a grade N42 Neodymium Iron Boron magnet. The magnet is 1 inch long and 3/16 of an inch in diameter. The outer diameter was chosen as it fit well in the endotracheal tubes used for this project. The size and grade were chosen from the optimal field strength for the previously selected GMR sensor. It was desired to have a magnet whose field strength over the predicted distance values would match the linear range of the sensor. For this magnet, the sensor will have a linear output from approximately 15 mm to 35 mm, with the sensor saturating at approximately 8 mm. This also works well with the calculated critical depth of 32.8255mm (~12 oersteds) as it is within the linear range of the sensor.

Selection of Other Parts

Output from the sensor was amplified using an INA216P instrumentation amplifier. This boosted the signal from 0 to 300 millivolts to 0 to 3.9 volts using an amplification of 13. While the DAQ used was capable of reading these values unamplified, it was desired to increase the voltage to ensure the device was compatible with low cost microcontrollers as well. The INA2126P was chosen for its low noise, high gain, low power draw, and ease of use. The one downside is that it requires a symmetric power supply. Because the desired operating voltage was approximately zero to 5 volt, a 10 volt power supply and voltage regulator were needed. The regulator used was a

29W1Q81 5-volt regulator. It was chosen for its low power consumption and stable output. The DAQ used for the project was a NI USB 6008, which interfaced with LabVIEW. Data from the DAQ was sampled at 100 Hz.

Full Design Construction

An image of the device prototype can be seen in Figure 15 along with the prototype's electrical diagram in Figure 16. The test platform has two GMR sensors attached to the breadboard through 1-foot wire leads. Two GMR sensors were used as it allowed for testing of two separate sensors without having to change hardware or rewiring the breadboard. The breadboard itself contains the instrumentation amplifier and its power supply. The 5-volt dc regulator powers a 5+, 5-, and 0-volt bus bar. This symmetric power supply was achieved by referencing the ground pin on the amplifier to the 5-volt pin on the voltage regulator. Output from the amplifier stage is wired to the USB-6008 DAQ along with the reference ground lead. Small drops of hot glue were used for strain relief to prevent leads from being pulled off the board during testing.

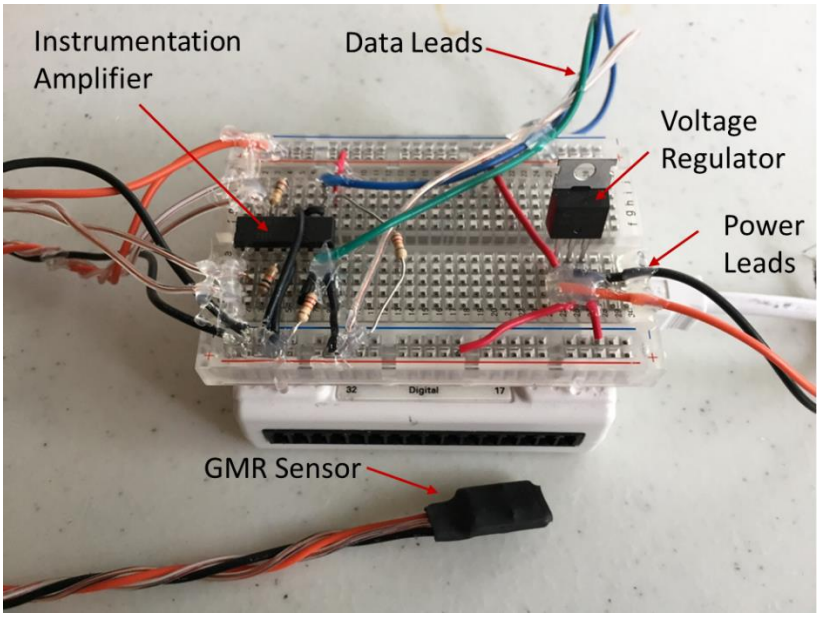

Figure 15. A picture of the prototype sensor, amplifier, and DAQ. The current prototype is laid out on a bread bored for ease of adjustment. The final design will be surface mounted in a single package.

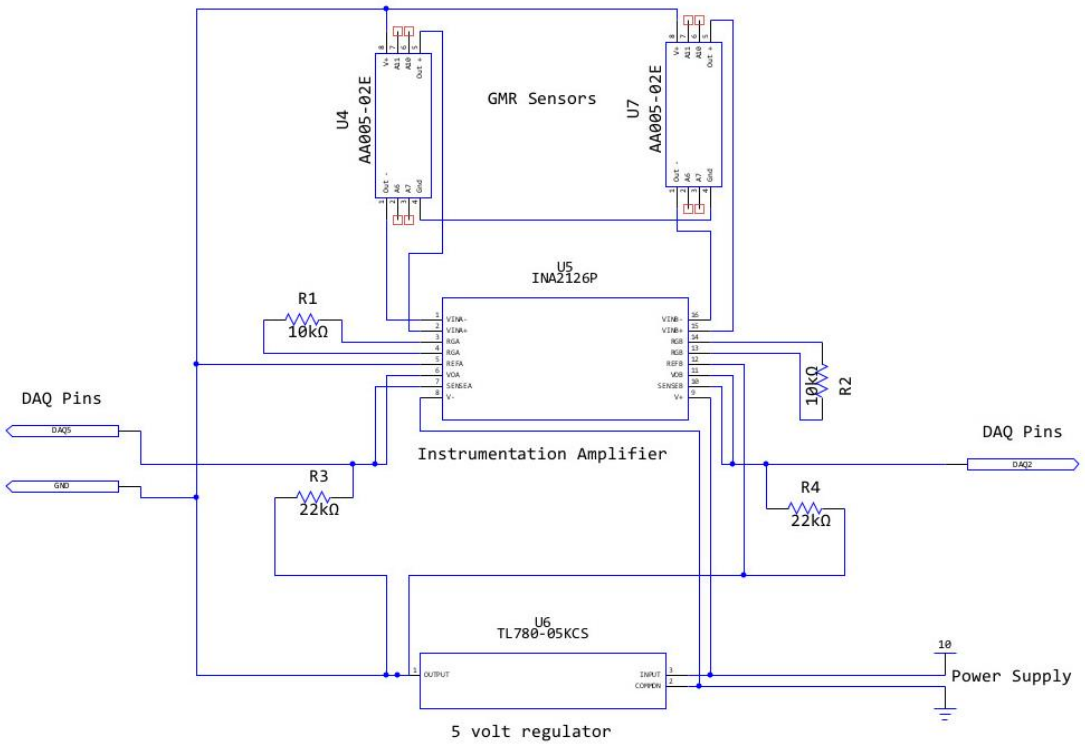

Figure 16. An electrical schematic of the sensors along with their connection to supporting hardware. The prototype sensor is made from two NVE AA005-02E GMR sensors. Output from the sensors is passed through an INA2126P Instrumentation amplifier with a nominal gain.

The other half of the design is the magnetic stylet. The magnetic stylet was made by clipping off the end of the plastic sheath of the stylet and stretching it over the K&J magnet. This effectively embedded the magnet in the end of the stylet. The stylet still has the same flexibility as a regular stylet allowing for proper shaping of the ET tube during the procedure. Figure 17 shows the stylet and magnet next to an ET tube.

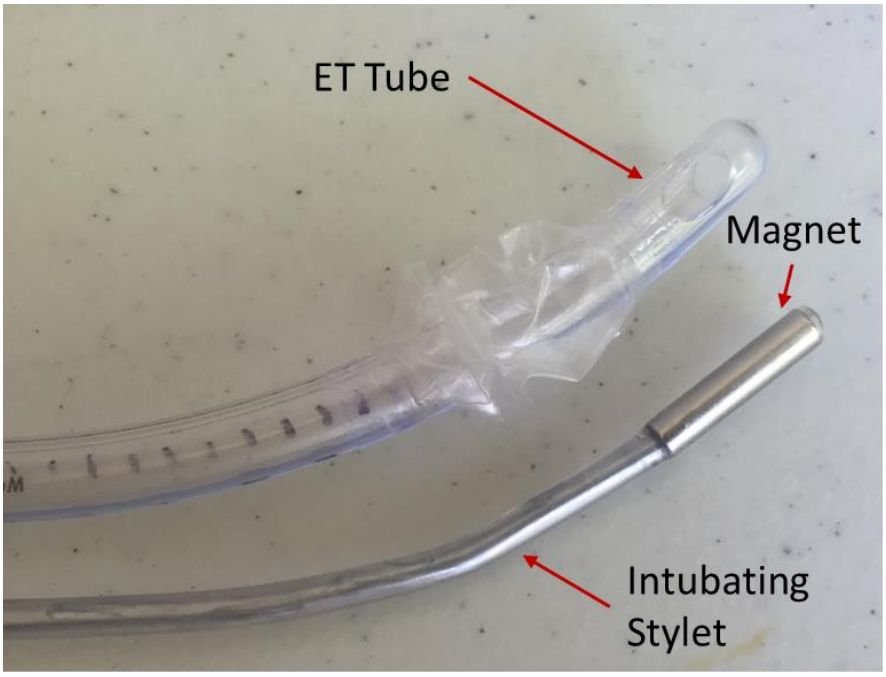

Figure 17. The tip of an ET tube next to the magnetic stylet made for this project. The magnet is embedded at the end of the stylet. The stylet goes inside the ET tube and provides support for the ET tube during the intubation procedure.

Equations

In order to build a functional sensor it is important to know the relationship between distance and the output of the selected GMR sensor. This allows for sensor calibration as well as analysis of error in the sensors output. For this project, two equations must be derived to create this model. The first is an equation that relates distances in millimeters to magnetic field strength in oersteds and the second relates this field strength to sensor output in millivolts.

The equations governing the relationship between magnetic field strength and distance are provided below in Equation 5. The magnetic induction outside a magnet is calculated by integrating the magnetostatic potential over the volume of the magnet. ρ and z are the radial and axial components of the field outside the magnet while R and Z are the length and radius of the cylindrical magnet. The F component of both equations can be set to zero, as the magnet is radially symmetric. μ_0 and M are the permeability of free space and the magnetization of the material, respectively [19].

$$\Phi_m(\rho, z) = \frac{\mu_0}{4\pi} M \int\int\int \frac{(z-Z)\, R\, dR\, d\Phi\, dZ}{\left[\rho^2 - 2R\rho\cos\Phi + R^2 + (z-Z)^2\right]^{3/2}} = \frac{\mu_0}{4\pi} M \left(\int\int \frac{R\, dR\, d\Phi}{\sqrt{\rho^2 - 2R\rho\cos\Phi + R^2 + (L/2-z)^2}} - \int\int \frac{R\, dR\, d\Phi}{\sqrt{\rho^2 - 2R\rho\cos\Phi + R^2 + (L/2+z)^2}} \right) \quad \textbf{(5)}$$

This equation can be simplified by assuming the cylindrical magnet is a pair of monopolar disks separated by a distance L (Equation 6.a & 6.b). In these equations ρ and z represent the radial and axial position outside the magnet. Since magnetic field strength is calculated at the center of the bar magnet (z=0), the B_p term goes to zero because the field lines of the magnet are all parallel to the axis of the magnet.

$$B_z = -\frac{\mu_0}{4\pi} M \int_0^{2\pi} \int_0^{a} \left(\frac{R\,(L/2-z)}{\left(R^2 + (L/2-z)^2 + \rho^2 - 2R\rho\cos\Phi\right)^{3/2}} + \frac{R\,(L/2+z)}{\left(R^2 + (L/2+z)^2 + \rho^2 - 2R\rho\cos\Phi\right)^{3/2}} \right) dR\, d\Phi \quad \textbf{(6.a)}$$

$$B_\rho = -\frac{\mu_0}{4\pi} M \int_0^{2\pi} \int_0^{a} \left(-\frac{R\,(2\rho - 2R\cos\Phi)}{2\left(R^2 + (L/2-z)^2 + \rho^2 - 2R\rho\cos\Phi\right)^{3/2}} + \frac{R\,(2\rho - 2R\cos\Phi)}{2\left(R^2 + (L/2+z)^2 + \rho^2 - 2R\rho\cos\Phi\right)^{3/2}} \right) dR\, d\Phi \quad \textbf{(6.b)}$$

It should be noted that while these equations can be solved numerically for specific values of magnet size and measurement distance, a general solution cannot be easily found; this problem has been documented in J.M Camacho and V. Sosa's paper on alternative methods for calculating magnetic fields of a permanent magnet [20]. These solutions take the form of an incomplete elliptical integral, which cannot be expressed in simple mathematical terms. Since the equations can be solved numerically with Mathematica, it was possible to create a plot of theoretical voltage outputs versus distance using the known parameters of the magnet being used for this project. This plot can be seen in Figure 18. Note that the plot includes the linear conversion factor from oersteds to voltage, which will be discussed in Equation 8. By calculating the values for field strength over the range of expected operating distances and fitting a curve to these points it becomes possible to approximate the relationship between field strength and distance; in this case a function of the form y=a*ln(x)^3+b*ln(x)^2+c*ln(x)+d. This form was chosen since the curve appears to take on the shape of an exponentially decreasing function. A third order polynomial is chosen as it is known that magnetic field strength decreases at approximately 1/x^3 with respect to distance. The

mathematic code used to generate the points for this curve can be found in Appendix A. The equation generated can be seen in equation 7.

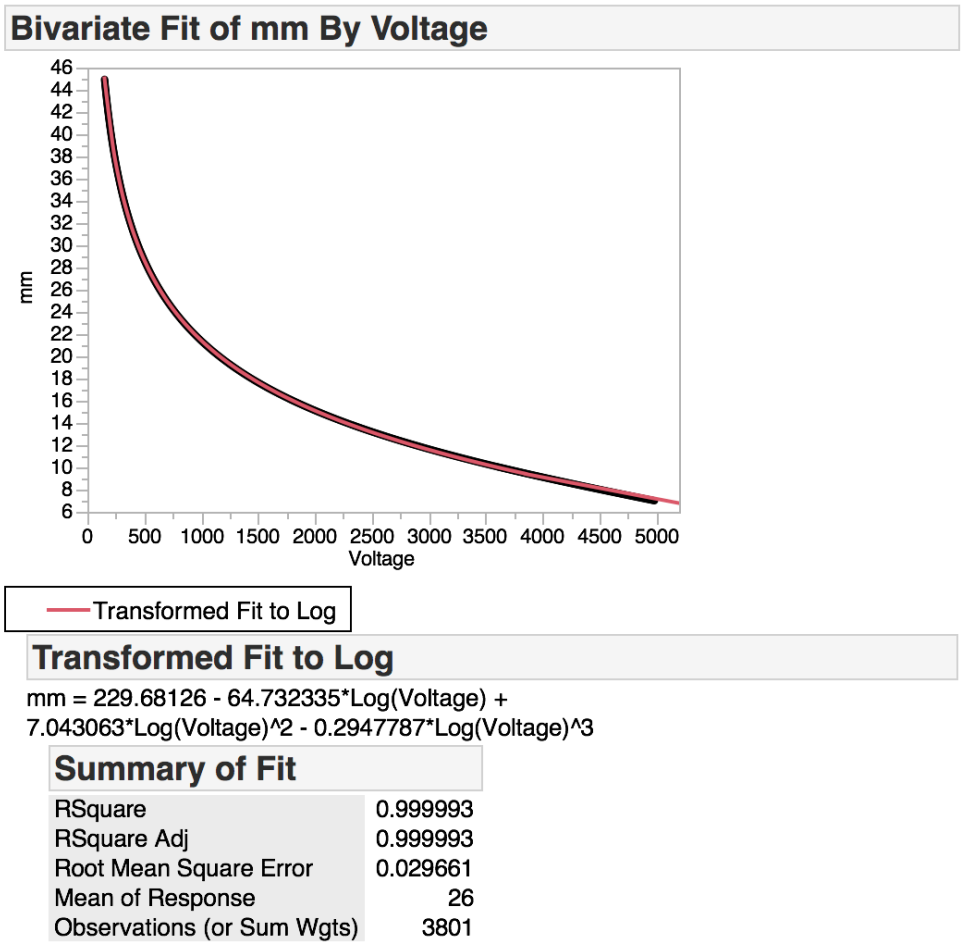

Figure 18. A fit model relating voltage to predicted distance. This model was found by numerically solving the Bz equation for specific points and then fitting a line to those points in SasJMP. This was done as the general solution to the Bz equation is mathematically difficult to find.

$$\boldsymbol{D = 229.6 - 64.73 * Ln(V_{out}) + 7.04 * Ln(V_{out})^2 - 2.94 * Ln(V_{out})^3} \qquad \textbf{(7)}$$

The next equation relates magnetic field strength to the voltage output of the GMR sensor. The chosen GMR sensors have a linear output between 10 and 70 oersteds, meaning that the relationship between field strength and voltage output can be determined by the linear relationship shown below in Equation 8. K is the sensor sensitivity, **B** is the field strength along the sense axis, Vin is the bridge voltage, and G is the gain of the amplifier. It should be noted that nominal values from the spec sheet were used during the calculation of the theoretical model. The values are 0.5

mv/v-Oe for k, 5 for Vin, and 13 for G. These values come from the sensor and amplifier selected in the previous section.

$$V_{out} = K * B * V_{in}*\mathrm{G} \quad (8)$$

Validation of Distance Model and Sensor Calibration

A validation test was performed on the sensor and magnet to see how the device's output compared to the theoretical model. Data from this test was also be used to derive the actual relationship between distance and millivolt output for a specific sensor. For this test, the cylindrical N42 magnet with a diameter of 3/16 inches and a length of 1 inch was taped to the end of a set of plastic dial calipers as seen in Figure 19. The magnet was purchased from K&J Magnetics. The GMR sensor tested was an NVE AA005-02E, with a linear range from 10 to 70 oersteds.

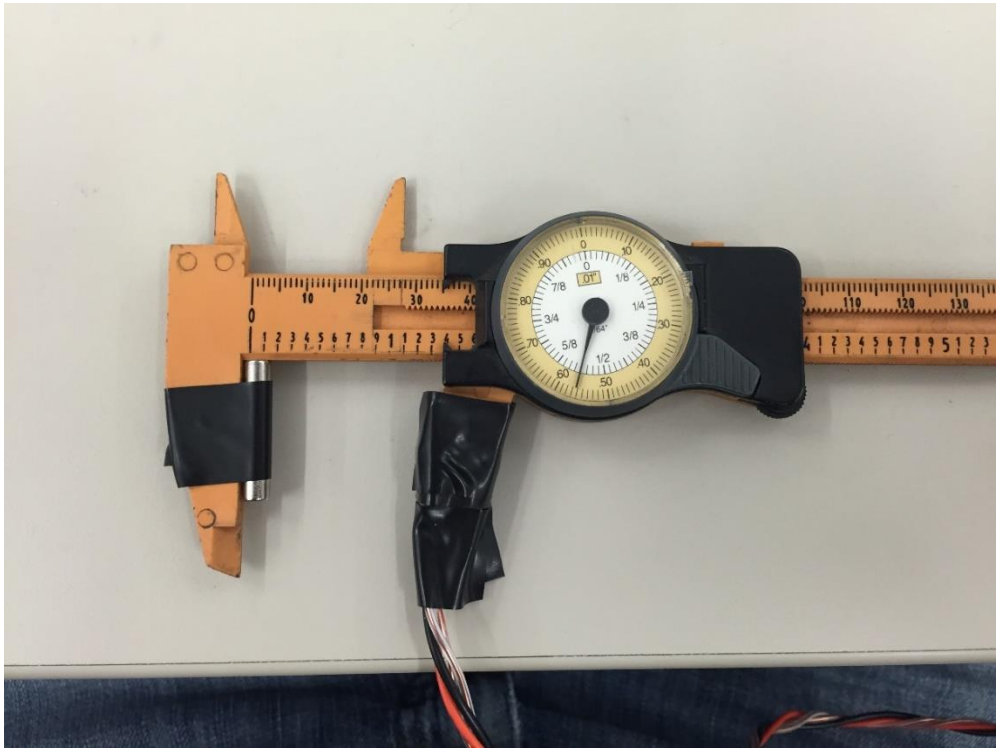

Figure 19. The testing rig for this experiment with magnet and sensor attached to the calipers. Voltage measurements were taken at 1mm intervals from 50 to 15 mm. Data from this test was used to derive a distance vs voltage output model for the specific sensor used in this test. The RMSE value from this model was then used to estimate sensor uncertainty.

The GMR sensor was then taped to the moving end of the dial caliper. The sensor element was aligned so that the sense axis was parallel to the N/S axis of the magnet. The sensor element

was fixed at the same height as the midpoint of the magnet. This was done to maximize the field strength in the direction of the sense axis of the sensor element. Figure 20 shows the sense axis of the sensor element.

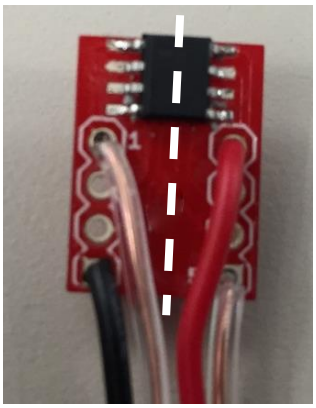

Figure 20. The white line represents the sense axis of the GMR sensor. Sensor output is maximized when the field lines are parallel to this axis.

To measure the distance versus sensor output, the sensor was slowly advanced toward the magnet. Measurements of voltage output were taken at 1 mm intervals from 50 mm to 15 mm. Since the theoretical model calculates distance from the z-axis of the magnet, the distances read from the calipers had to be converted into the separation distance between the magnet and sensor. This was done by subtracting the measured distance at zero separation then adding the radius of the magnet. In this case, the separation distance was 8 mm and the radius of the magnet was 2.38mm.

The voltage outputs from this test were then compared to the predicted values from the ideal model derived in the previous section to determine how closely these models compare. Then a non-linear regression was performed on the data to create a model from the measured data. This used the same non-linear third order approximation as the theoretical model. The RMSE value of this regression was used to calculate the overall error in the calibrated sensors. A sensitivity analysis was also performed on the sensor model to assess how changes in certain sensor parameters affected the output of the sensor.

Validation of Sensor and Magnetic Field Model

Figure 21 shows the plot of millivolt output vs measured distance along with the non-linear regression model generated from the data. The full statistical summary of this model has been included in Appendix B. While the fit shows a high R^2value and a low RMSE error, it should be

noted that the residuals were somewhat heteroscedastic. This comes from the fact that the nonlinear model fit to the curve is not an exact representation of the physical model. This model also assumes that all the error exists in the sensor and that the distance measurements are accurate. This assumption is only partially true as the dial calipers used in the test are not perfectly accurate.

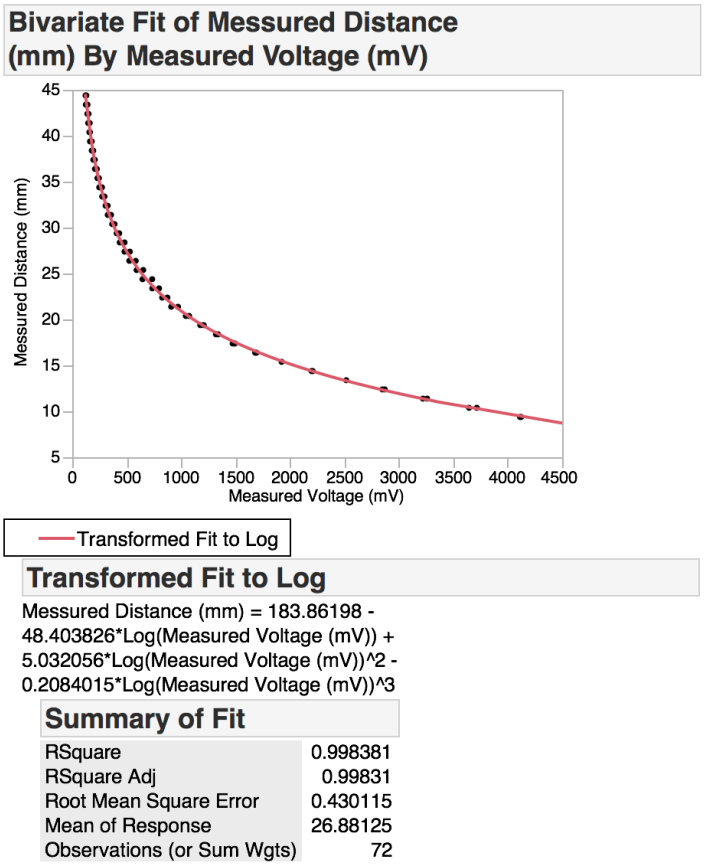

Figure 21. The SasJMP fit model of the measured voltage vs the measured distance during the sensor validation test. The model fit to the data had an R^2 value of .998 with a standard deviation of 0.43. This means that the sensor can measure distances with a certainty of $\pm$ .86mm

This model indicates that the RMSE error or standard deviation of the predictor model is 0.43mm. This means that this sensor and amplifier configuration have an uncertainty of ±.86mm when predicting a distance from a measured voltage using this model. In order to ensure that this uncertainty does not lead to false positive indication of tracheal intubation, it is necessary to subtract this uncertainty from the calculated critical distance. This ensures that at the maximum deviation from the predicted model the device will not indicate tracheal intubation when esophageal intubation is present. This leads to the final critical distance of 31.5mm. This critical distance gives a threshold of 336 millivolts or 10.3 oersteds.

The measured distances were also compared to the distances predicted by the theoretical model to see how well the measured values matched with the theoretical values. The plot of this comparison can be seen in Figure 22. The analysis in SasJMP shows that the theoretical model is a good predictor of sensor output with a root mean square error of .56mm. It should be noted that not all of this error is sensor noise, as some of the error originates from the fact that the theoretical model is itself an approximation of the true magnetic field model.

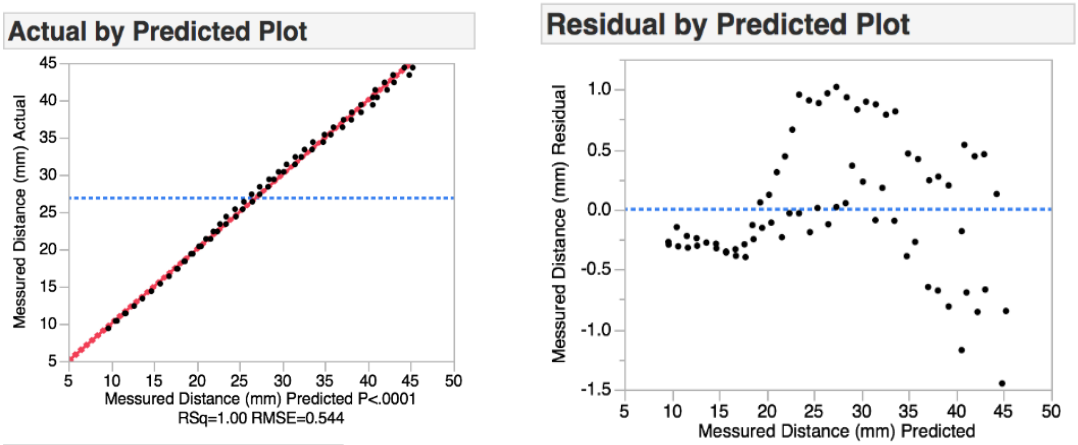

Summary of Fit

RSquare	0.997334
RSquare Adj	0.997296
Root Mean Square Error	0.543977
Mean of Response	26.88125
Observations (or Sum Wgts)	72

Figure 22. The actual-by-predicted plot and the residuals from the comparison of the measurements and theoretical model. The heteroscedasticity in the residuals come from the fact that there is some inherent error in the theoretical model as it is itself an approximation of the incomplete elliptical integral that defines magnetic field strength vs distance.

A sensitivity analysis was also performed on the data to assess how variability in sensor parameters and noise effect the sensor output. These variables include parameters such as sensor sensitivity, temperature offset, and gain error in the amplifier. These uncertainties were added to the previously derived model to give an equation that relates distance to voltage output with error. Each value was changed while the other values were left fixed to assess the effects changing one uncertainty value would have on the overall output. A list of the values tested along with their effects on the sensor can be found in table 1. The Mathematica code used to perform the analysis can be found in Appendix C.

***Table 1**. Sensitivity Analysis Results: Nominal Distance of 35.63*

Sensor Parameter	Nominal Value	Range	Distance	%Dif of nominal
Sensitivity mv/v-Oe	.5	±.15	32.24mm	9.8%
Power Supply Voltage	5v	±.1	35.34	.8%
Hysteresis	0	%4	30.12	15%
Angle	0 degree	10 degree	35.83	.56%
Bridge offset	0 mV	±4	33.432	6.168%
Temperature	23C	±5	34.74	2.49%
Gain Error	0	.02%	35.63	0%
Amplifier offsets	0µV	.1	35.65	0%
Resistor	10kOhm	±.5	36.01	10%
DAQ Noise	0mV	±4.28	35.43	3%

The sensor parameters that had the highest effect on sensor output were variations in sensor sensitivity, bridge offset voltage in the sensor, variation in the resistance of the gain resistor, and hysteresis in the sensor. Fortunately, bridge offset voltage, sensor sensitivity, and gain resistor uncertainty only effect the sensor-to-sensor error, not the measurement error. This is because these values are properties of the sensor and amplification circuit. This means that the sensor can be calibrated to remove the effects of these errors.

Hysteresis and temperature were the only two variables that showed a significant effect on sensor performance that could not be calibrated out of the system. Hysteresis is not seen to be a problem as the sensor is only concerned with measurements during the insertion procedure and will not be reading tube position when the sensor is being removed. As the sensor is mounted to the surface of the neck, it is expected to be at a constant temperature of 98.7F degrees with little variation during the procedure.

Chapter 4. Plastic Mockup Testing and Results

This chapter will provide an overview construction and testing procedures for the plastic mockup test rig. First, it will discuss why a plastic mockup was chosen for testing. Next, it will discuss the construction of the mockup and the parameters used to size the simulated anatomy. Finally, it will discuss the tests performed on the mockup and the result of these tests.

Plastic Mockup Construction

One of the main challenges with this project was the construction of an accurate testing analog for the human upper airway. While cadaver testing or other real world biological testing would have been ideal, access to and restriction on these types of tests meant that such methods were beyond the scope of this project. As such, an accurate human body analog was needed. One easy solution was the use of pig tracheas and esophagi. These organs are cheap and easy to obtain from local slaughterhouses. The porcine model is useful for testing because the shape and location of a pig's upper airway is very similar to that of a human. While useful, pig tracheas are somewhat difficult to work with as they must be cleaned and thawed before each test. Therefore it was necessary to create an easy access tracheal model for performing distance measurements and calibrations.

Using human neck anatomy data the following tracheal model was constructed. Built from PVC and flexible Tygon tubing it represents a patient with a 14 inch neck circumference and a representative tracheal wall-to-neck surface thickness of 11.1mm (6.4mm PTT). Wall-to-neck surface thickness represents the total distance from the inner wall of the simulated trachea to the surface of the neck. For these experiments, the tracheal wall thickness will be assumed to be 4.7mm with the rest of the simulated surface to neck thickness representing pre-tracheal tissue thickness.

The mockup is built from of a 3/4 inch inner diameter PVC pipe wire-tied to a 3/4 inch Tygon tube. PVC was chosen to simulate the rigid properties of the trachea, while Tygon was chosen to simulate the flexible nature of the esophagus. Both PVC and Tygon tubes have a magnetic permeability close to 1.0. Wire ties were used as the help to flatten out the Tygon tube to better simulate the shape of the esophagus. The PVC pipe has an inner diameter of 20.52mm, which is very close to the calculated mean inner tracheal diameter. The minimum separation between the simulated esophagus and trachea is 6.1 mm which is only slightly higher than the

documented esophageal thickness mean of 5.26 mm [17]. As the simulated neck only covers half the simulated trachea's length, the device can be used to simulate wall to neck surface thickness of as low as 3.3 mm (0 PTT).

The two inner tubes were attached to the inside wall of the 4 inch tube used to simulate the surface of the neck. The primary use of the simulated neck surface was to test the effects of angular displacement from the midline of the neck on the sensor's ability to detect proper intubation, as well as whether or not multiple sensors could be used to increase the accuracy of the system. 2 mm foam shims were used to simulate a variety of wall to neck surface thickness from 3 mm (0mm PTT) all the way out too 18 mm (13.3mm PTT) in thickness. The sensor is fixed to the outside of the rig with either tape or another non-permanent adhesive. Marks were made at 10 cm from both ends of the test rig to facilitate measurement of depth versus tube placement as well to as ensure consistency between tests. 10 cm was chosen as the endotracheal tube used in the test has a mark at 10 cm from its end. This means that at an insertion depth of 10mm the tip of the tube should be directly under the sensor. An image of the mockup model with the senor attached can be seen in the Figure 23.

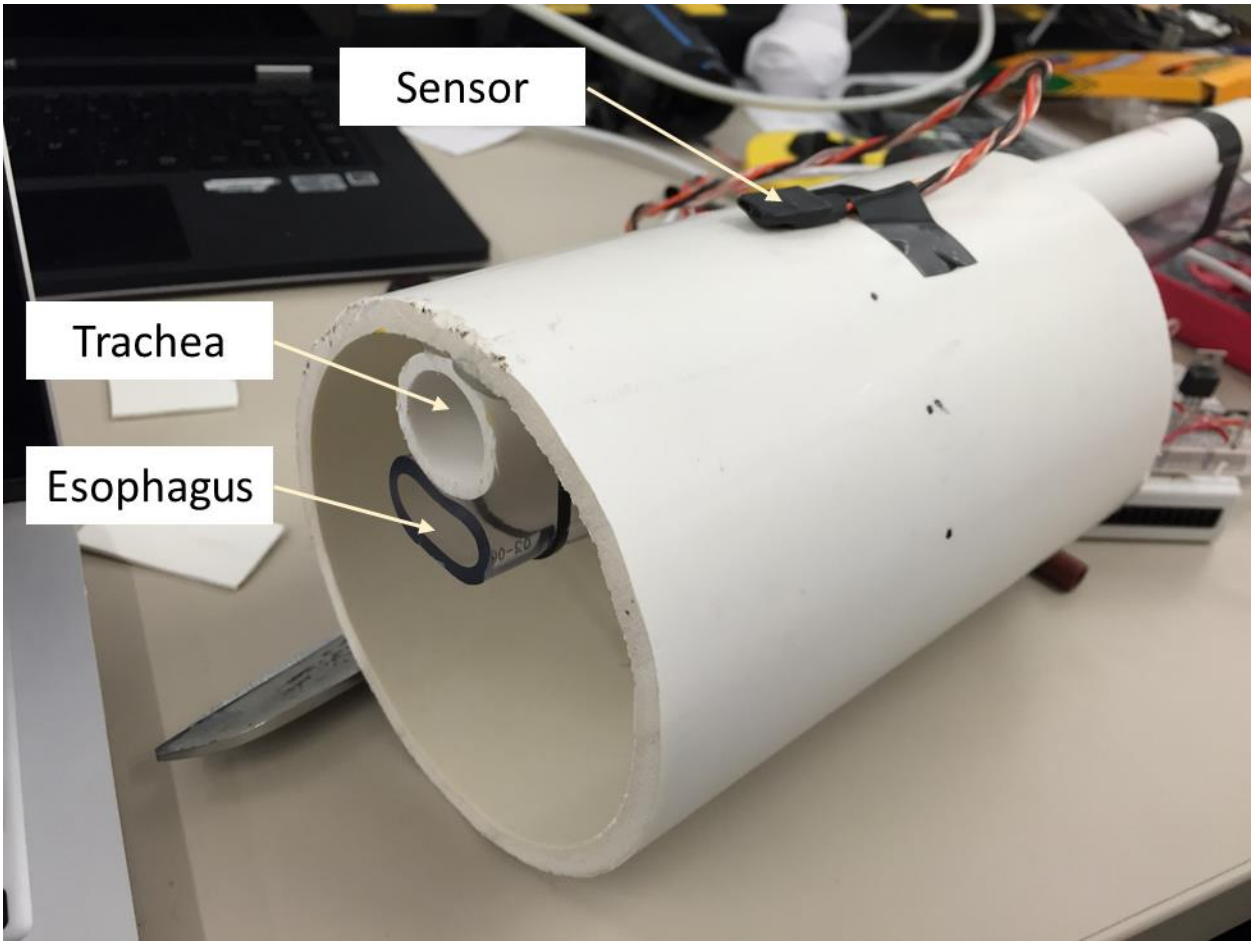

Figure 23. Image of the test rig with sensor mounted to the center of the tube. Tape holding the sensor has been removed to allow for better visualization.

Mockup Testing and Results

Several tests were performed on the mockup to provide information about sensor performance. The primary test on this setup was the evaluation of the calculated critical depth that would indicate esophageal intubation. This was done by measuring signal strength versus surface depth for multiple levels of simulated subcutaneous fat and assessing how the sensor performed. Data from this testing was compared with the result from the pig trachea testing to validate the mockup model.

Depth vs Output at Multiple Wall to Neck Surface Thickness Testing Procedure

For this test, the sensor was mounted 10 mm below the entrance to the PVC trachea and esophagus. The sensor itself was fixed so that it sat on the midline of the tube parallel to the plane

separating the esophagus and the trachea. The sensor was aligned so that the sense axis was parallel to the vertical axis of the tubes. Pre-tracheal tissue was simulated with 2 mm thick craft foam placed between the PVC tube and the sensor. This foam plus the thickness of the PVC walls was summed to give the total simulated thickness. For this test wall to neck surface thickness of 3, 5, 11, 15, and 18mm were tested.

After the sensor was mounted, the magnet was attached to the end of the stylet and inserted into the endotracheal tube. For these tests, the tube was marked at 5mm intervals from 6 cm to 15 cm. This test used the edge of the PVC pipe as the measurement baseline. The 5mm interval was feasible because the baseline for this test was much sharper, making it easier to take precise distance measurements.

For this test, three measurements were taken for each thickness. The first measurement assessed the sensor output with the tip ET tube tilted toward the front of the trachea. This was achieved by tilting the tube back levering the tip forward. The second measurement assessed the sensor output with the tip toward the back of the trachea. This was achieved by bending the tube forward, causing the tip to lever backwards. These tests not only helped assess sensor performance but also helped to examine the variability of emitter positions inside the trachea. A final set of measurements were taken with ET tube in the simulated esophagus.

Depth Versus Output at Multiple Tracheal Wall-to-Neck Surface Thicknesses Results

The results from the insertion depth versus output test on the mockup showed that the sensor performed well. The sensor successfully detected tracheal intubations in wall to neck surface thicknesses of up to 18mm. However, at 18mm it was only indicated briefly, with a max sensor output of 344.5 millivolts. This functional distance is slightly lower than expected. This may indicate that the ET tube trends more toward the back of the trachea, which could affect the usability on patients with higher PTT thicknesses. Figure 24 shows the output of the sensor at minimum and maximum wall-to-neck surface thickness at which the device functions.

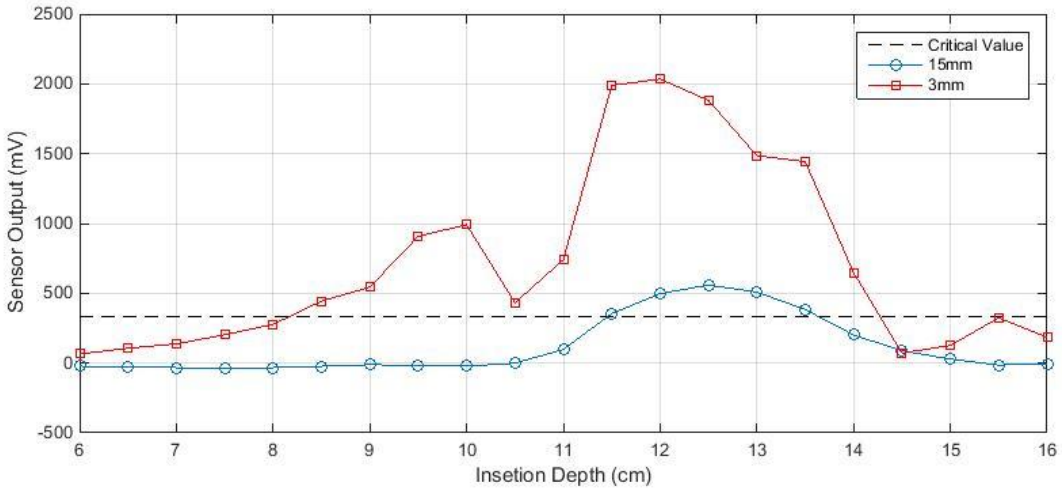

Figure 24. This graph shows the sensor outputs at the minimum and maximum wall to neck surface thicknesses at which the device functions.

The main effect that the pre-tracheal tissue thickness had on sensor output apart from magnitude was the range of tube insertion lengths at which the device would indicate tracheal intubation. At 3.3mm, the device indicated tracheal intubation from an insertion length of 85mm to 140mm while at 15mm it indicated tracheal intubation from an insertion length of 120mm to 130mm. This mainly affects the usability of the device, as the longer the sensor output is above the threshold, the easier it is to read the indicator. At high pre-tracheal thicknesses, the binary indicator may only briefly flash on and off, which may lead to the indication being missed. One possible solution to this problem may be to include multiple magnets in the stylet to increase the range of insertion lengths at which the tube can be detected.

Angular Displacement Testing Procedures

The next set of tests assessed the effects that angular displacement from the midline of the neck had on sensor output. It was hypothesized early in the design process that having multiple sensors in a circumferential array would prove to be more accurate than a single point sensor. This test was used to see if this hypothesis was correct or not. It was also useful in parameterizing how the sensor performed if it was misplaced or otherwise not installed correctly.

The same procedure holds for this test as the previous two insertion depth versus output tests. The sensor was attached to the surface of the PVC pipe section that simulated neck circumference. The PVC pipe was marked at 2.54, 5.08, and 7.62 cm intervals off the midline of the tube. The sensor was then attached to the tube with tape and aligned so that the sense axis was

parallel to the vertical axis of the pipe. Like before the intubation tube was inserted at .5 cm intervals from the 6 cm mark on the tube to the 15 cm mark on the ET tube. After each test, the sensor was moved to a new angular location and the test was repeated. The same procedure was repeated for esophageal intubation. Figure 25 shows the sensor mounted at an offset from the midline of the neck.

Figure 25. The test setup for evaluating the effects angular displacement has on sensor output. It was theorized that by visualizing the trachea an esophagus from the side would allow for an alternative method of assessing tube placement.

Angular Displacement Results

The angle test demonstrated that there is little benefit at this time to adding multiple sensors in an array configuration. As the distance from the midline increases the sensor, output decreases for both the trachea and esophagus. It was hoped that by placing a sensor on the side of the neck that it would be closer to the esophagus and thus provide a higher output then the midline sensor during esophageal intubation; however, this was not the case. Multiple sensors may prove useful

in the future but as of this iteration, they do not improve the device's function. Figure 26 shows the output at different angles for tracheal and esophageal intubations at a fixed PTT.

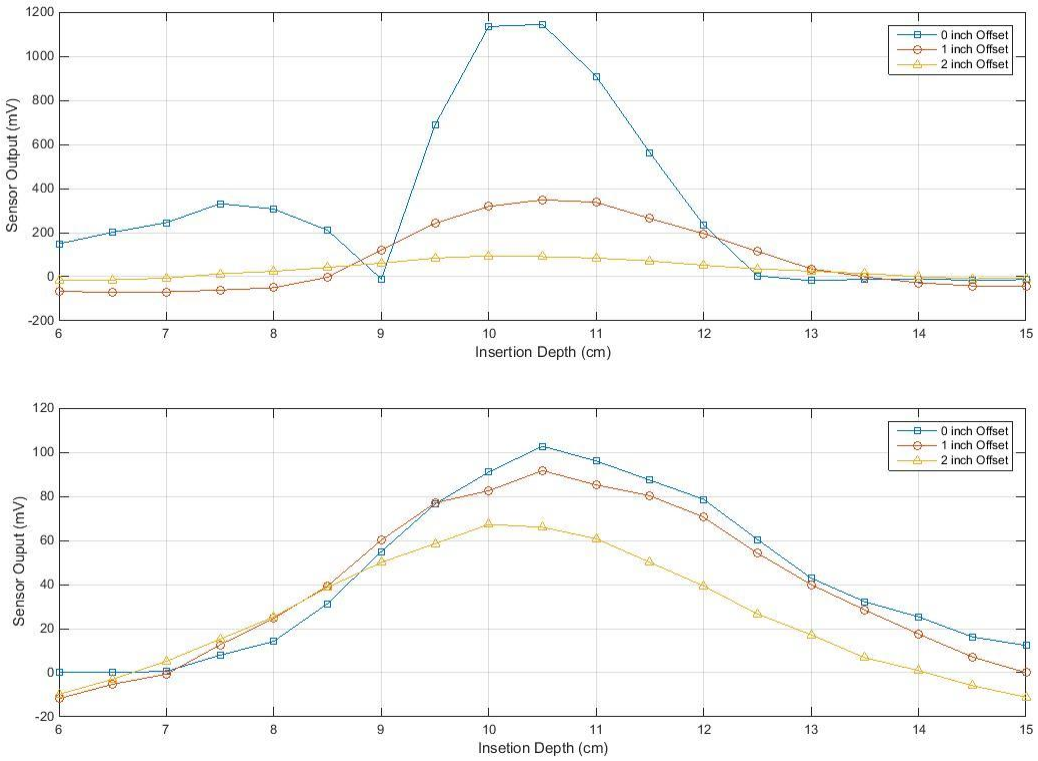

Figure 26. Tracheal (top) and esophageal (bottom) signal outputs for 11mm of wall to neck surface thickness at different angles. At higher offset angles both the tracheal and esophageal outputs decrease.

Chapter 5. Pig Trachea Testing and Results

This chapter will provide an overview construction and testing procedures for the porcine model test. First, it will discuss why a porcine model was chose for testing and why it is a suitable model for this project. Next, it will discuss the construction of the porcine model testing rig and the procedures used to perform test. Finally, it will discuss the testing preformed on the porcine model and the results of those test.

Pig Trachea Testing Rig Construction

In order to validate this sensor, it is necessary to test on a realistic anatomical model along with a mock-up. Ideally, these tests would be performed on live patients or human cadavers, but due to time constraints and IRB restriction, this was not possible. One easy-to-implement alternative to these anatomical testing models were pig tracheas. Pig tracheas are roughly the same size and very close in shape to human tracheas. Pig tracheas are often used during airway management and crycothrotomy training for this very reason. They are easy and inexpensive to obtain and they require no IRB approval to use. The pig tracheas for this project were obtained with the help of Dr. Robertson from the Biomedical Engineering and Sciences department at Virginia Tech.

The pig trachea model used in this test served two main purposes. The first was to validate the PVC model and demonstrate that the values measured on the mockup were similar to a real anatomical model. The second was to perform a full anatomical validation of the sensor in as close to a real intubation as possible. The pig anatomy used for this test consisted of the entire upper airway of the pig along with its esophagus. This included the entire larynx, the epiglottis, and the trachea all the way to the carina. These anatomies were chosen, as they would cover most of the major airway landmarks used in intubation. The tongue and upper jaw were not included, as it would have greatly increased the difficulty of test with little benefit to data quality. While a pig trachea can only approximate a human airway, the data collected from these test proved to be an excellent starting point for validation and future research on the sensor.

The pig tracheas needed to be cleaned and prepped before testing. Because the trachea came from a slaughterhouse, certain extra anatomy needed to be removed. The major arteries, veins and their connective tissue were removed as they impeded sensor placement. A large portion of the thyroid was also removed as it hindered access to upper airway markings. The carina and

the lower portion of the airway were removed to facilitate mounting of the trachea and to allow for internal measurement of the tracheal diameter. The pre-tracheal fascia above the first and second tracheal rings was cut in order to expose the tracheal cartilage below. This was done to create a clean, dry place to mount the sensor to the trachea itself.

The trachea was mounted to a simple wooden test stand. This stand kept the trachea vertical in order to simulate a human neck as well as prevent pressure on the esophagus. The stiff larynx was lightly wedged between the two wooden uprights with lateral pressure provided by a set of elastic bands. The slight compressive force combined with the natural friction of the fascia held the trachea in place. Although the organ experienced lateral compression neither the esophagus nor the trachea were effected as the airway was held open by the rigidity of the laryngeal cartilage. Figure 27 shows the test rig. Note the cleaned portion below the cricoid, circled in red.

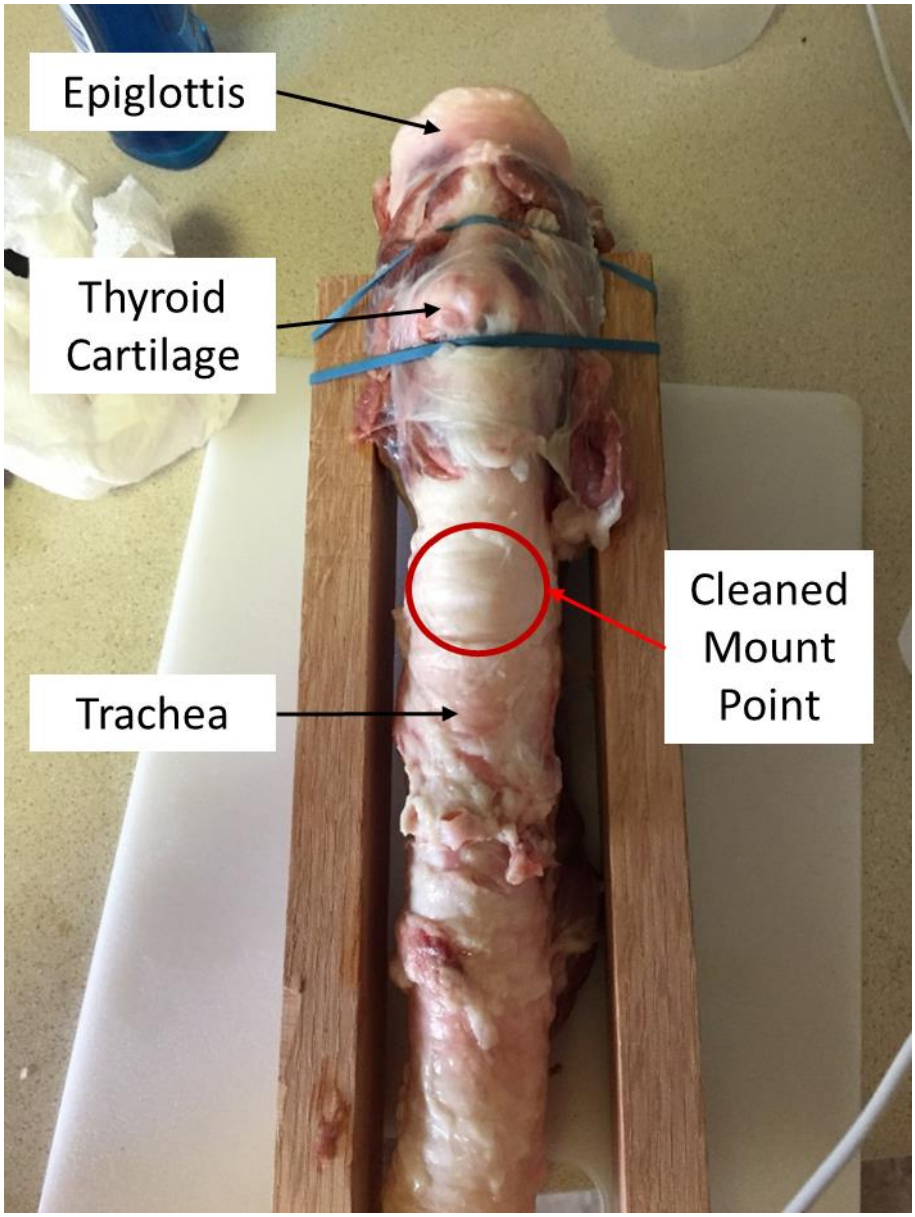

Figure 27. The trachea was held in place with rubber bands around the thyroid cartilage. The thyroid cartilage holds the airway open so that no pressure is applied to the trachea or the esophagus when the organ is mounted this way.

In addition to supporting the trachea, a method for advancing the ET tube at fixed intervals was needed. This was achieved by building a small PVC gantry and pulley system that could be used to lower the tube into the trachea and hold the tube steady during measurements. As seen in Figure 28, the ET tube was suspended from monofilament wire counter balanced with a small weight. The weights and the friction of the wire kept the tube at a fixed height during measurements, helping to reduce error. Marks were made on the monofilament wire at 5mm intervals to help assess tube insertion depth.

Figure 28. The gantry system for supporting and advancing the ET tube through the pig trachea. The ET tube is suspended by monofilament line attached to a counter weight. Marks on the monofilament line are used to assess insertion depth.

Pig Trachea Testing Procedure

The primary test carried out on the pig trachea was an evaluation of the sensor's performance on as close to a real anatomical model as possible. Data from this test was also used to validate the PVC mockup model. This test simulates the passage of an ET tube through the throat and into the trachea of the patient. It measures the depth of insertion versus signal output of the sensor. The curve generated by this data can be used to validate both the function of the device and the PVC mockup. The distance versus output measurement helped establish the function of the sensor while the shape of the curve generated during tube passage can be used to verify qualitatively the mock up model.

The first step in testing was mounting the sensor to the trachea. Padding was taped to the sensor element to simulate sub-cutaneous fat and skin. For this test, a pre-tracheal tissue thickness of 6mm was used. The sensor was then glued to the cleaned surface of the trachea just below the second tracheal ring. The sensor was aligned so that the sense axis was parallel to the vertical axis of the trachea. Cyanoacrylate glue was used as it provided a strong bond to the surface of the

trachea and ensured that the sensor remained relatively immobile with relation to the anatomy. Next, the endotracheal tube was prepped by inserting the stylet into the tube with the tip of the magnet resting just below the murphy eye. The tube used for this test was a Mallinckrodt 7.5 mm ET tube. The stylet was then fixed in place using electrical tape to prevent the magnet from sliding with relation to the tube. A mark was made on the epiglottis at the top of the false vocal cords to act as a baseline for the measured insertion depth. Unlike the plastic mockup, there is no clear delineator to the start of the trachea. This is a minor issue as it only affects the offset of the maximum signal output and not the actual magnitude of the signal. Markings were placed on the tube at 1cm intervals to act as a guide for depth measurement. Measurements were taken using LabVIEW and the USB 6008 DAQ. Measurements of the inner diameter of the trachea were taken with a set of plastic dial calipers at the carinal end of the trachea. Figure 29 shows the pig trachea with the sensor mounted.

Figure 29. Trachea with the sensor attached. The sensor and foam spacers are held onto the trachea with. Cyanoacrylate glue. This glue was chosen as it allows the sensor to be fixed to the trachea without applying pressure on the airway or esophagus.

After the sensor was attached and the tube was prepared the hardware was turned on and data recording began. For the first test, the epiglottis was pulled back and the tube was inserted past the vocal cords and into the trachea. The tube was advanced at 10 mm intervals with measurements taken each time a mark on the tube aligned with the mark on the epiglottis. The signal strength from the GMR sensor was measured from a depth of 10 cm of tube insertion to 19 cm. Figure 30 shows the intubation of the pig trachea with the measurement baseline indicated.

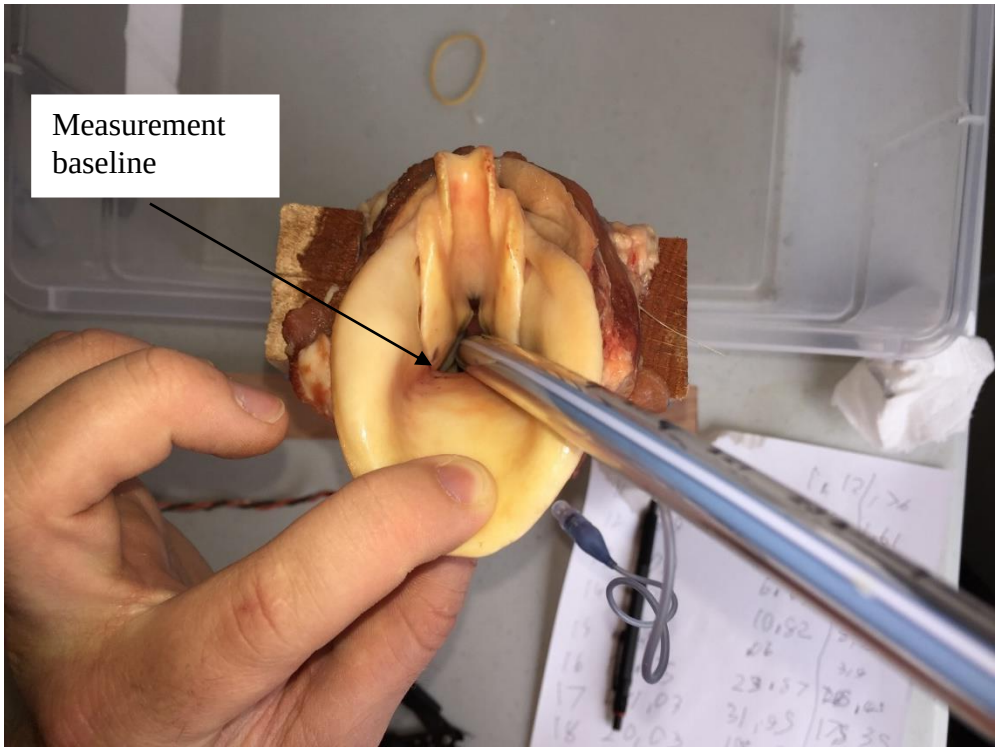

Figure 30. Insertion of the intubation tube and magnetic stylet through the epiglottis and into the trachea. Measurements of sensor output were taken at 1 cm intervals of insertion depth from 10cm 19cm of tube length.

The procedure was then repeated for esophageal intubation. For this test, the entrance to the esophageal lumen was used as the distance baseline as it was at approximately the same height as the mark on the epiglottis. Again, data was recorded from 10cm of insertion depth to 19 cm of insertion depth. It should be noted that during both tests, the ET tube was aligned with the midline of the trachea. It is shown offset in these images to facilitate visualization of the anatomy. Figure 31 shows the esophageal intubation being performed.

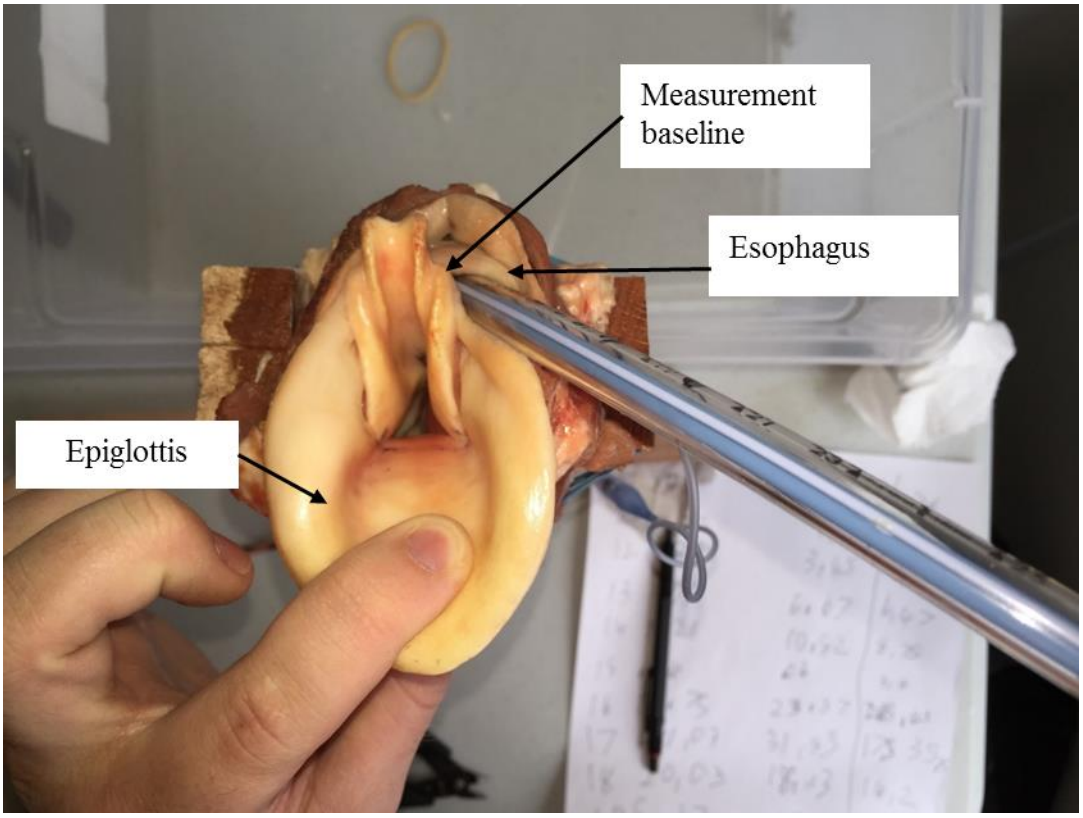

Figure 31. Insertion of the intubation tube and magnetic stylet into the esophagus. Again, measurements were taken at 1cm intervals for 10cm to 19cm.

A third intubation test was performed without the epiglottis. Because of the unique shape of the porcine epiglottis, it was difficult to accurately read markings on the tube with relation to the baseline mark. Oftentimes the epiglottis had to be manipulated slightly to visualize the marks, but doing so would change the lateral distance of the tube inside the pigs' trachea. This caused the readings to jump around making it difficult to determine the correct sensor output. By cutting a hole in the membrane, the top of the thyroid cartilage could be used as a stable, easy-to-read baseline. While less anatomically accurate, this method produced data values that were much more repeatable. This third test was also much more similar to the PVC test since the plastic mockup does not simulate the epiglottis. Figure 32 shows the intubation being performed through the cricothyroid membrane.

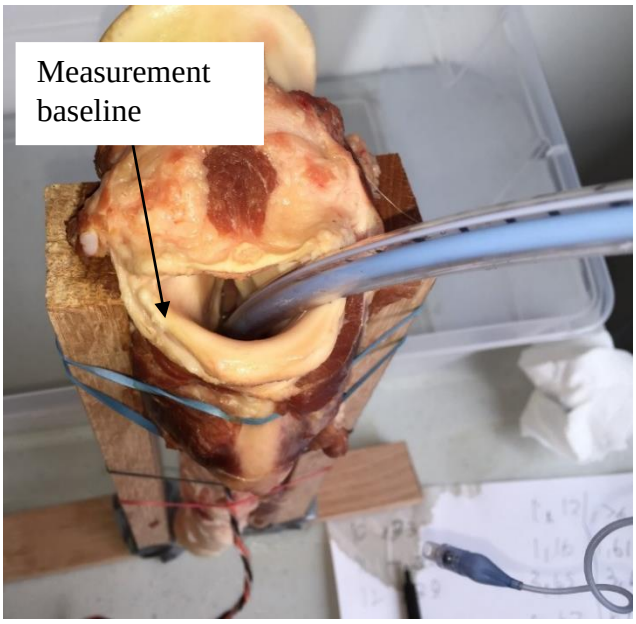

Figure 32. Intubation preformed without the epiglottis. The porcine epiglottis interfered with tube positioning during measurement due to its large shape. Although less anatomically accurate, this configuration provided more consistent results.

A final test was performed later in the design process using the gantry discussed earlier. After analysis of the data from the initial three intubations, it was felt that the data lacked enough fidelity to draw a suitable conclusion. The gantry was used to advance the tube at 5mm intervals through the trachea and allowed for much more stable sensor output. This also ensured that esophageal and tracheal measurements would have the same distance baseline. Several different pre-tracheal thicknesses were simulated using foam padding. As in the previous test, the trachea was intubated through the membrane between the epiglottis and the thyroid cartilage since the large size of the pig's epiglottis interfered with the wire used to lower the ET tube. A measurement of sensor output versus time during the simulated intubation procedure was also taken. This returned high-resolution curves, which were useful for qualitative comparison of the mockup model with the tracheal model. A figure of an intubation being performed with this gantry system can be seen in Figure 33.

Figure 33. The pig trachea and gantry used to lower an ET tube into the trachea. The gantry system was used as it provided results that are more consistent than previous manual insertion tests. The ET tube is suspended from monofilament wire and held in place with a counter weight. Marks on the wire allow for the tube to be advanced at precise 5mm intervals allowing for more accurate measurements of distance versus output.

Validation of Mock Up and Pig Trachea Tests

Measurements from the first three pig trachea tests proved to be of limited use. The 10mm insertion depth interval, coupled with the inaccuracies caused by inserting the tube by hand, resulted in data that was of limited usefulness. This lead to the creation of the gantry system discussed earlier which allowed for a much higher degree of control when inserting the ET Tube.

Measurements on the pig trachea were taken with the gantry at distances of 4mm, 8mm, and 12mm of wall-to-surface thickness. The device performed well during these tests indicating tracheal intubation at all three distances with no false positives during esophageal intubation. However, while the shape of the curves generated from the pig trachea test were the same as those found in the mockup, the signal strengths were different. The output from the pig trachea was somewhat higher in all cases. This is unexpected as the pre-tracheal distance measurements for the pig trachea are slightly thicker than the mockup's. It was also found that the maximum values from

the pig trachea did not follow the same pattern as the mockup model. In the mock up-model maximum signal strength decreased as pre-tracheal tissue thickness increased, while in the pig model the 4mm thickness showed lower max values then the 8mm thickness by 10 oersteds. Figure 34 shows a plot of two pig tracheal tests compared to the mockup tests at similar PTTs. The graphs show some discrepancy in the measured values but curves with the same general magnitude and shape.

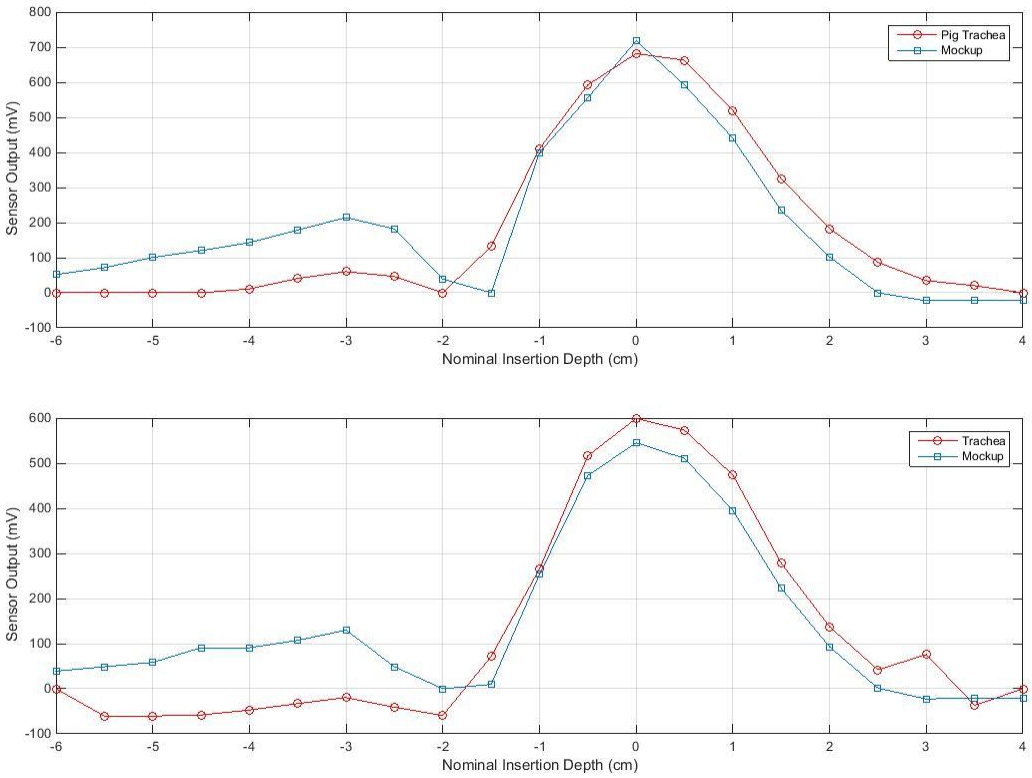

Figure 34. Overlay plots of the Sensor output versus Normalized Insertion Depth for two different sets of tests. The zero point corresponds to the point where the magnetic emitter is directly beneath the sensor. Both tests show similar curve patterns as the magnetic stylet passes the sensor, but the magnitudes are slightly different.

These discrepancies are believed to be due to the fact that the pig trachea is both wider and more flexible than the PVC mockup. In the PVC mockup, the ET tube is somewhat constrained as to where it can be inside the simulated trachea. The cuff and the stiffness of the stylet tend to keep the ET tube tip relatively close to the center of the trachea. The diameter of the pig trachea is much larger than that of the ET tube, meaning that its position can vary substantially inside the trachea. That, coupled with the lack of bone and supporting tissues, leads to measurements with a higher degree of variability.

Despite the differences in magnitudes, the device preformed adequately, indicating true tracheal intubation during all tests, and not indicating tracheal intubation during esophageal intubation. However, the pig tracheal diameter of 35mm was somewhat larger than the predicted human tracheal diameter of 20.25mm. This means that the esophagus in the pig trachea was significantly farther away from the sensor than predicted, making the pig trachea an unsuitable model for examining false positive cases. This indicates that further validation on more accurate models, such as a cadaver, is needed.

Qualitative Curve Test

To assist in the validation of the PVC mockup, a qualitative test was performed to visualize the output signal strength as the endotracheal tube passed the sensor. This test measured signal strength versus time of a tube being passed through the trachea at an arbitrary velocity. The goal of this test was to provide a qualitative view of the sensor response in both the mockup and the anatomical model. This is useful as it provides a higher resolution curve than those produced by discrete sample tests, making it easier to visualize the motion of the ET tube.

The setup for this test was the same as the previous sensor output versus depth tests. Again, the sensor was secured to the surface of the PVC mockup and the pig trachea. Instead of sampling, the output at discrete distance intervals data from the sensor was continuously sampled. The ET tube was then inserted into the simulated trachea and the pig trachea at a slow and steady rate, while the output of the sensor was plotted on a graph. The curve produced by this graph was then saved for future analysis. This test was performed on both the pig trachea with a simulated wall to neck surface thickness of 6 mm and the mockup with a simulated thickness of 7 mm.

Qualitative Curve Results

The qualitative curves, which recorded high-resolution plots of signal output versus time during the insertion of an ET tube, show similar patterns between the pig trachea and the mockup. What this demonstrates is that the anatomy of the pig trachea does not create a substantial different insertion path for the tip of the tube. If the anatomy was substantially different from the mockup, the shape of the curve should also change. While only a qualitative comparison, it provides validity to the claim that the mockup is a suitable model for testing. Figure 35 shows the overlay plot of these two qualitative tests.

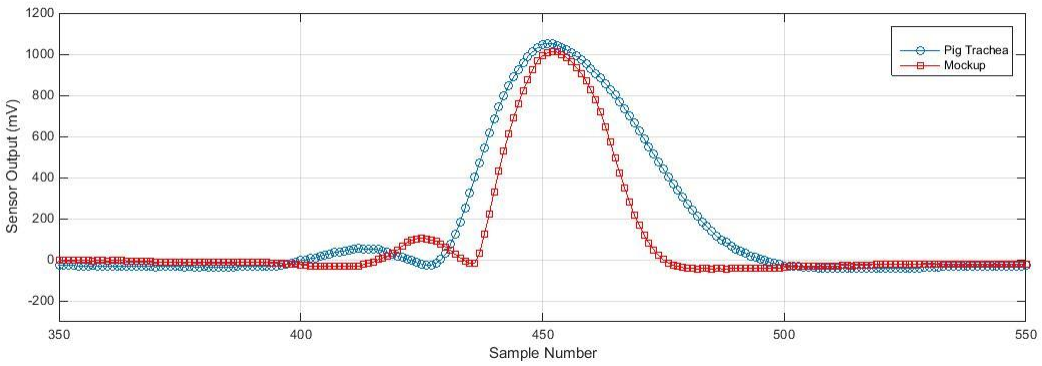

Figure 35. Sample number (Time) versus sensor output for the mockup and pig trachea qualitative curve tests at 6mm of pre-tracheal tissue thickness. The data is presented over a 200 sample range for each of the respective tests. Both curves show similar curve shapes and magnitudes providing a qualitative assessment of the mockup with relation to the pig trachea.

Chapter 6. Usability Testing, Conclusions, and Future Research

This section will cover the overall conclusions and future goals of the project. First, it will look at the qualitative performance test preformed on an intubation dummy. Then, it will look at the current and predicted usability of the device along with some areas that require further testing. Next, it will look at some improvements to be made to the device to prepare it for further development. Finally, it will lay out the future goals of the project.

Intubation Training Mannequin Testing

Near the end of the study, a brief opportunity arose to test the sensor on an intubation training mannequin. This head and torso dummy simulates the upper airway trachea and esophagus as well as other important anatomy for intubation. The goal of this test was to provide more insight into the functionality of the device in a full throat system. A major advantage of this dummy was that it allowed for the entire intubation procedure to be simulated instead of a single part of the process. It should be noted that the training dummy's throat anatomy varies somewhat from a normal human trachea as it contains some extra training aids. The main difference is that there is a hole in the trachea at the cricothyroid membrane. Despite these discrepancies, data from this test was still valuable as it allowed for an assessment of the sensor in an accurate representation of the intubation procedure.

For this test, the sensor was fixed to the midline of the neck just below the cricoid cartilage. The sensor was aligned so that its sense axis was parallel to the vertical axis of the trachea. Before taking measurements, the skin of the neck was pulled back and the depth to the trachea was measured. It was found that the dummy has a pre-tracheal tissue thickness of 18mm, which was somewhat higher than predicted values. One of the doctors present was then asked to use the provided intubation tube and stylet to perform an intubation on the mannequin. Sensor output was monitored and recorded using the LabVIEW software. Notes were also taken on how the doctor interacted with the device and whether or not it interfered with the procedure. Next, the mannequin was intubated with the tube just past the cords, well above the sensor position. Using the front of the teeth as a baseline the tube was slowly advanced down the trachea with measurements of sensor output taken at 1cm intervals. Figure 36 shows the intubation training mannequin during the intubation and data collection procedure.

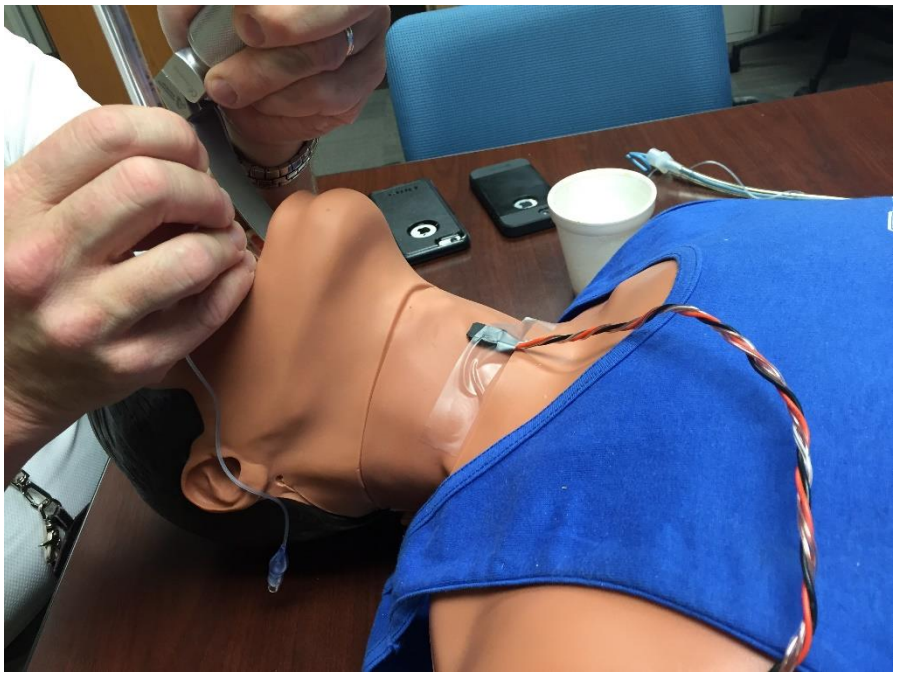

Figure 36. Testing was performed on an intubation training mannequin at Wake Forest University Baptist Medical Center. This test was designed to both assess the sensor in another anatomical model as well assess how the sensor performed in an accurate representation of an intubation procedure.

Intubation Training Dummy Testing Results

Testing on the intubation dummy provided some very promising results. From this test, it was found that the device functioned and was minimally disruptive to the current intubation procedure. Tube manipulation and insertion were the same as the non-automated intubation method. The magnetic stylet did not interfere with the procedure and passed smoothly over the chosen laryngoscope blade. Sensor placement on the neck was out of the way of the intubating physician, despite the fact that wires were present. One major result of this testing was confirmation that tube passage could be monitored during the procedure. During all typical intubation attempts, the doctors were able to watch the tube pass the sensor during the procedure, confirming the functionality of the real time monitoring aspect of this project.

Magnitudes of the recorded sensor values were in line with the predicted output values at the estimated pre-tracheal tissue thickness between 15mm and 18mm, with a peak value 14.25 oersteds and a vertical detection range of 3cm. Two failure modes were observed during testing. The first occurred when the patients head was tilted forward. This appears to pull the tube farther back in the trachea increasing the distance from the surface of the neck. This position of the neck

is not optimal for intubation as it obstructs the airway. By tilting the head back to the proper position, the signal returned to values above the threshold. The other failure mode detected was a false positive indication of tracheal intubation when pressure was applied to the sensor. This was done to simulate the effects the Sellick maneuver would have on the sensor output. Because pressing on the sensor causes it to move closer to the esophagus preforming the Sellick maneuver is not recommended when using this device. This should not be a problem, as according to the doctors at Wake Forest, the Sellick maneuver is falling out of favor and can therefore be safely avoided when using this device.

Overall, the doctors at Wake Forest were impressed with the prototype and were excited to see further testing of the device. They also had several suggestions and concerns that they would like to see addressed. The first was the need to ensure safe performance in patients with atypically thin necks. The doctors also brought up the need for a more compact and ergonomic sensor package. They stated that they would prefer a single unit device that his held against the surface of the neck instead of one that uses adhesive sensors. They felt that this would speed up the assessment process and reduce potential interference from sensor wires. Finally, they suggested adding multiple magnets to the stylet. This would allow for tracking of the whole ET tube instead of just the tip of the tube.

Device Functionality and Use Case

The functionality of this device is expected to expand as further iterations are developed. Currently, the device is suitable for use in adult male patient with a waist circumference less than 120cm and greater than 77.9 cm. As of this iteration, the device is not suitable for use in adult women as the female trachea is an average of 14cm, which is different enough from the male tracheal diameter to warrant a change in set point. This is one of the first problems that should be addressed in the next iteration. This iteration is also not recommended for children and young adults under the age of 20, as there is a large variation in tracheal diameter with age, rendering a fixed set point invalid. With the current design, it is also advised that caution be used when operating on atypically thin patients. While the currently selected sensor set point is, design to work with 99.7% of the population's esophageal distances there is still a chance that a thin patient may deviate enough from the norm to cause issues.

This device is not intended to replace current intubation detection methods but to provide another level of verification. It should be used in conjunction with other methods of tube placement confirmation such as end tidal CO_2. No one method is guaranteed to work all the time, so multiple verification steps are needed to ensure proper tube placement. However, unlike other methods it can be used to verify tube position during the intubation procedure.

Because the device uses magnets, there are several specific cases where its use is not recommended or where further testing is needed to verify its safety. The first case is in the event that a patient has an implanted pacemaker or defibrillator. These devices specifically state that they should not be exposed to strong external magnetic fields. As the trachea passes very close to the heart, an intubation with a magnetic stylet may not be safe for these devices. This interaction will need to be studied during further iterations of the project, but as of now, the use of this device near pacemakers is not recommended.

Another case occurs when intubating patients with body modifications. Ferrous piercings in the tongue and soft tissue of the neck have the potential to be attracted to the magnet on the end of the intubating stylet interfering with the procedure or acting as a pinch point. This is thought to be a less serious issue as most piercings can be easily removed and often are removed before an intubation procedure. Along with piercings, this device is not recommend for use in patients with injuries from shrapnel or embedded metal.

Future Device Development

A number of improvements can be made to the device to improve its usability, while preparing it for the small business innovation research grant process (SBIR). The first and most important is to allow the device to be used in adult women. This will require a new set point to be derived for the average tracheal diameter of the adult female population. Making this change will be simple, though it will require its own set of test to validate the new device.

Along with improving and expanding the usability of the device to work with adult females, it is also important to address the functionality of the device in obese patients. While the device should function satisfactorily in 85% of the population, it is not predicted to work well in the 15% of the population with the highest pre-tracheal tissue thickness. One possible solution is performing a study on the pre-tracheal tissue thickness of populations with similar weights. Using this data, it should be possible to create more accurate estimates for esophageal distance, as the

data would only look at a portion of the total population. This data could then be used to create a series of devices for use in different weight ranges, with one device used for thinner patients and another used for obese patients.

The set points can be further refined by performing a study on available MRI data from medical record archives. This IRB approved study would look at MRI data of patient's necks to measure the relevant tracheal and esophageal distances directly. With a large enough sample size, it should be possible to create two statistically meaningful data sets: one for esophageal distances and one for tracheal distances. These data sets should have less uncertainty than the estimated distances calculated in this paper, as they will only look at a single distance instead of the sum of several distances. This could also be used to help find relevant correlations between easily measurable anatomical features, such as neck circumference and pre-tracheal tissue thickness, allowing for further refinement of the critical distance based on patient size.

Another improvement that will need to be made is to the device construction and interface. Currently, the sensor is attached to the device hardware via wires, which is then read and displayed on a computer. The next iteration of the design will integrate the sensor, microcontroller, and indicator lights into one small handheld device. Instead of the sensor being attached to the neck with medical adhesive, the new device will be held to the midline surface of the neck. This will simplify the use of the device, as it will only need to be placed on the surface of the neck to function. Feedback from the device will be integrated into the unit with both light and sound indicators providing clear information to the user. The stylet will also be modified to contain magnets along its entire length. This will allow for tracking of the stylet throughout the entire procedure as well as continuous monitoring of tube position in the throat.

Conclusion

Over the course of this project, a great deal of progress has been made towards the development of a functional automatic esophageal intubation detector with many of the stated project goals being met. An automated assessment of ET tube placement should reduce the risk of undetected esophageal intubation by providing feedback about the procedure unclouded by physiological state or operator experience. By measuring the distances from a patient's neck to the tracheal wall, this assessment was based solely on patient anatomy. Using a GMR sensor and a magnetized stylet, it was possible to create a sensor that met this need while still being inexpensive

and proved to be easy-to-operate. This design also helped minimize changes to the current intubation procedure and proved easy to operate during simulated intubation procedures. The prototype developed is accurate and has been able to successfully identify tracheal intubation in several simulated environments with only one instance of a false positive, which occurred in an atypical use case. As false positive indication of tracheal intubation is never acceptable, these results are very promising especially for a first prototype.

While the results are very promising, they also indicate the need for further testing. An important part of parameterizing a device's function and usability is identifying when and where the device fails. With so little data on false positive failure rate, it becomes difficult to perform this critical part of the validation process. In order to solve this problem, the device needs to be tested and validated on a human upper airway. As the device is not ready for live testing, this next round of testing will have to be performed on a cadaver model. Cadaver models are useful, as they will provide an accurate human airway model without the need as strict IRB approval. In addition, the cadaver model will more accurately reflect the material properties of the tissue. A cadaver is more flexible then the PVC mockup and contains the supporting bone and tissue missing from the pig tracheal model. One shortcoming with the test performed during this study was the fact that they could not simulate the flexibility of the esophageal wall, which may affect tube position inside the throat. Ideally, the device will be tested on several different cadavers to give a range of body types and pre-tracheal tissue thicknesses.

This testing will take place in collaboration with the Wake Forest University Baptist Medical Center anatomy lab in Winston Salem. Ideally, this will happen during the airway training course in July. Data from these tests and the research conducted during this project will be used to develop the next iteration of the design. This design iteration will be used for writing an SBIR research proposal, which will seek to develop the final version of the device and start human trials.

References

[1] R. Walls and M. Murphy, *Manual of Emergency Airway Management*. Wolters Kluwer Health, 2012.

[2] K. C. Dittrich, "Delayed recognition of esophageal intubation," *Can. J. Emerg. Med.*, 2002.

[3] A. Timmermann, S. G. Russo, C. Eich, M. Roessler, U. Braun, W. H. Rosenblatt, and M. Quintel, "The Out-of-Hospital Esophageal and Endobronchial Intubations Performed by Emergency Physicians," *Anesth. Analg.*, vol. 104, no. 3, 2007.

[4] H. E. Wang, G. K. Balasubramani, L. J. Cook, J. R. Lave, and D. M. Yealy, "Out-of-hospital endotracheal intubation experience and patient outcomes.," *Ann. Emerg. Med.*, vol. 55, no. 6, pp. 527–537.e6, Jun. 2010.

[5] M. D. J. E. Fiadjoe, M. D. H. Gurnaney, M. D. N. Dalesio, B. A. E. Sussman, P. D. H. Zhao, M. S. X. Zhang, and M. D. P. A. Stricker, "A Prospective Randomized Equivalence Trial of the GlideScope Cobalt® Video Laryngoscope to Traditional Direct Laryngoscopy in Neonates and Infants," *Anesthesiology*, vol. 116, no. 3, pp. 622–628, 2012.

[6] R. E. O'Connor and R. A. Swor, "Verification of endotracheal tube placement following intubation," *Prehospital Emerg. Care*, vol. 3, no. 3, pp. 248–250, Jan. 1999.

[7] B. A. MacLeod, M. B. Heller, J. Gerard, D. M. Yealy, and J. J. Menegazzi, "Verification of endotracheal tube placement with colorimetric end-tidal CO2 detection," *Ann. Emerg. Med.*, vol. 20, no. 3, pp. 267–270, Mar. 1991.

[8] W. BOZEMAN, D. HEXTER, H. LIANG, and G. KELEN, "Esophageal Detector Device Versus Detection of End-Tidal Carbon Dioxide Level in Emergency Intubation," *Ann. Emerg. Med.*, vol. 27, no. 5, pp. 595–599, May 1996.

[9] M. T. Denton, "Intubation detection system with transducer based indicator." Google Patents, 1999.

[10] S. H. Akerson, "Tracheal intubation monitoring apparatus and method." Google Patents, 1994.

[11] D. Lederman, S. Lampotang, and M. Y. Shamir, "Automatic endotracheal tube position confirmation system based on image classification--a preliminary assessment.," *Med. Eng. Phys.*, vol. 33, no. 8, pp. 1017–26, Oct. 2011.

[12] NVE Corporation, "Application Notes," 2015. [Online]. Available: http://www.nve.com/SensorApps.php.

[13] J. F. Schenck, “The role of magnetic susceptibility in magnetic resonance imaging: MRI magnetic compatibility of the first and second kinds.,” *Med. Phys.*, vol. 23, pp. 815–850, 1996.

[14] O. R. Hung, “Clinical trial of a new lightwand device (Trachlight) to intubate the trachea,” *Anesthesiol.*, vol. 83, no. 3, pp. 509–514, 1995.

[15] E. Breatnach, G. C. Abbott, and R. G. Fraser, “Dimensions of the normal human trachea.,” *AJR. Am. J. Roentgenol.*, vol. 142, no. 5, pp. 903–6, May 1984.

[16] R. S. Hospital, “OSSEOCALCINEUS METAPLASIA VENTRO - DORSAL MEASUREMENT OF THE THICKNESS OF,” pp. 78–82, 2010.

[17] F. Xia, J. Mao, J. Ding, and H. Yang, “Observation of normal appearance and wall thickness of esophagus on CT images,” *Eur. J. Radiol.*, vol. 72, pp. 406–411, 2009.

[18] C. Szeto, K. Kost, J. a. Hanley, A. Roy, and N. Christou, “A simple method to predict pretracheal tissue thickness to prevent accidental decannulation in the obese,” *Otolaryngol. - Head Neck Surg.*, vol. 143, no. 2, pp. 223–229, 2010.

[19] S. M. Blinder, “‘Magnetic Field of a Cylindrical Bar Magnet,’” *Wolfram Demonstrations Project*, 2011. [Online]. Available: http://demonstrations.wolfram.com/MagneticFieldOfACylindricalBarMagnet/. [Accessed: 05-Jan-2015].

[20] J. M. Camacho and V. Sosa, “Alternative method to calculate the magnetic field of permanent magnets with azimuthal symmetry,” *Rev. Mex. Fis. E*, vol. 59, no. 1, pp. 8–17, 2013.

Image Citations

All images are by the author unless noted otherwise.

“For all photographs and images contained in the ETD either permission for use has been obtained or they have been evaluated, according to the four ‘fair use factors’ for copyrighted materials and deemed to be fair.

Figure 1 Page 6 [used with permission]
"Blausen 0872 UpperRespiratorySystem" by BruceBlaus. Blausen.com staff. "Blausen gallery 2014". Wikiversity Journal of Medicine. DOI:10.15347/wjm/2014.010. ISSN 20018762. - Own work. Licensed under CC BY 3.0 via Wikimedia Commons - https://commons.wikimedia.org/wiki/File:Blausen_0872_UpperRespiratorySystem.png#/media/File:Blausen_0872_UpperRespiratorySystem.png

Figure 2 Page 7 [Public Domain]
"Gray956" by Henry Vandyke Carter - Henry Gray (1918) Anatomy of the Human Body (See "Book" section below)Bartleby.com: Gray's Anatomy, Plate 956. Licensed under Public Domain via Wikimedia Commons - https://commons.wikimedia.org/wiki/File:Gray956.png#/media/File:Gray956.png
Public domain determination attached. [Work is public domain as it was created in 1918]

Figure 3 Page 8 [used with permission]
"Larynx external en" by Olek Remesz (wiki-pl: Orem, commons: Orem) - Own work, modified SVG version of PD picture from Gray's Anatomy.. Licensed under CC BY-SA 2.5-2.0-1.0 via Wikimedia Commons - https://commons.wikimedia.org/wiki/File:Larynx_external_en.svg#/media/File:Larynx_external_en.svg

Figure 4 Page 10 [used with permission]
"Sondeintubation" by bigomar2 - Self-photographed. Licensed under CC BY-SA 3.0 via Wikimedia Commons - https://commons.wikimedia.org/wiki/File:Sondeintubation.jpg#/media/File:Sondeintubation.jpg

Figure 5 Page 10 [used with permission]
"Tracheal tube stylet" by DiverDave. Licensed under CC BY 3.0 via Wikimedia Commons - https://commons.wikimedia.org/wiki/File:Tracheal_tube_stylet.JPG#/media/File:Tracheal_tube_stylet.JPG

Figure 6, Left Page 11 [used with permission]
"Macintosh Blades" by Sasata (talk) - I (Sasata (talk)) created this work entirely by myself.. Licensed under CC BY 3.0 via Wikipedia - https://en.wikipedia.org/wiki/File:Macintosh_Blades.jpg#/media/File:Macintosh_Blades.jpg

Figure 6, Right Page 11 [used with permission]
"Laryngoscopes-Miller blades" by User:DiverDave. Licensed under CC BY 3.0 via Wikimedia Commons - https://commons.wikimedia.org/wiki/File:Laryngoscopes-Miller_blades.JPG#/media/File:Laryngoscopes-Miller_blades.JPG

Figure 9 Page 21 [public domain]
"Endotracheal tube colored" by PhilippN - Modification of http://commons.wikimedia.org/wiki/Image:Endotracheal_tube_inserted.png. Licensed under Public Domain via Wikimedia Commons –
Public domain determination attached. [Work is public domain as it is a United States patent illustration]
https://commons.wikimedia.org/wiki/File:Endotracheal_tube_colored.png#/media/File:Endotracheal_tube_colored.png

Figure 10 Page 23 [from journal article]
J. F. Schenck, “The role of magnetic susceptibility in magnetic resonance imaging: MRI magnetic compatibility of the first and second kinds.,” *Med. Phys.*, vol. 23, pp. 815–850, 1996.

Figure 11 Page 24 [public domain]
"Gray384" by Henry Vandyke Carter - Henry Gray (1918) Anatomy of the Human Body (See "Book" section below)Bartleby.com: Gray's Anatomy, Plate 384. Licensed under Public Domain via Wikimedia Commons - https://commons.wikimedia.org/wiki/File:Gray384.png#/media/File:Gray384.png
Public domain determination attached. [Work is public domain as it was created in 1918]

Figure 13 Page 23 [public domain]
"Endotracheal tube colored" by PhilippN - Modification of http://commons.wikimedia.org/wiki/Image:Endotracheal_tube_inserted.png. Licensed under Public Domain via Wikimedia Commons –
Public domain determination attached. [Work is public domain as it is a United States patent illustration]
https://commons.wikimedia.org/wiki/File:Endotracheal_tube_colored.png#/media/File:Endotracheal_tube_colored.png

Appendix

Appendix A. Mathematica Code for Calculating Field Strength vs Distance

The code below was used to numerically solve for the predicted field strengths at different distances.

```
a = 0.00238125; (*Radius M*)
L = .0254;(*Length M*)
z = 0; (*Z postion of sensor M*)
ρ = Range[7, 45, .01] / 1000 (*Range of Distance from magnet to be tested mm*)
u = 4 π * 10 ^ - 7; (*Permiablity of Free Space N/A^2*)
M = 1.31 / (4 * π * 10 ^ -7); (*Magnitzation in Guass with conversion to SI*)

Oste = 10 000 u / (π * 4) * M * NIntegrate[ R * (L / 2 - z) / (R^2 + (L / 2 - z)^2 + ρ^2 - 2 * R * ρ * Cos[𝚹])^3/2 + R * (L / 2 + z) / (R^2 + (L / 2 + z)^2 + ρ^2 - 2 * R * ρ * Cos[𝚹])^3/2, {R, 0, a}, {𝚹, 0, 2 π}]

Data = {{ρ, Oste}};
```

Appendix B. Summary Statistics for Distance vs Field Strength Measurements

SasJMP fit summary for measured sensor output vs measured distance from the sensor validation test.

Bivariate Fit of Messured Distance (mm) By Measured Voltage

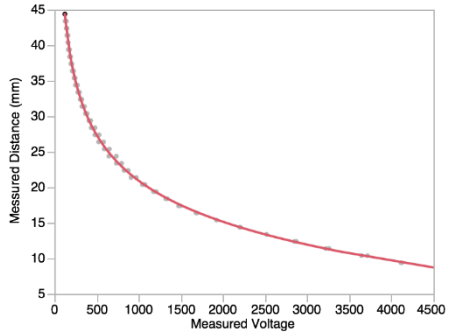

Transformed Fit to Log

Transformed Fit to Log

Messured Distance (mm) = 183.86198 - 48.403826*Log(Measured Voltage) + 5.032056*Log(Measured Voltage)^2 - 0.2084015*Log(Measured Voltage)^3

Summary of Fit

RSquare	0.998381
RSquare Adj	0.99831
Root Mean Square Error	0.430115
Mean of Response	26.88125
Observations (or Sum Wgts)	72

Lack Of Fit

Source	DF	Sum of Squares	Mean Square	F Ratio
Lack Of Fit	67	12.079935	0.180298	0.3606
Pure Error	1	0.500000	0.500000	Prob > F
Total Error	68	12.579935		0.8995
				Max RSq
				0.9999

Analysis of Variance

Source	DF	Sum of Squares	Mean Square	F Ratio
Model	3	7757.4201	2585.81	13977.41
Error	68	12.5799	0.18	Prob > F
C. Total	71	7770.0000		<.0001*

Parameter Estimates

Term	Estimate	Std Error	t Ratio	Prob>|t|
Intercept	183.86198	15.49338	11.87	<.0001*
Log(Measured Voltage)	-48.40383	7.298034	-6.63	<.0001*
Log(Measured Voltage)^2	5.032056	1.129972	4.45	<.0001*
Log(Measured Voltage)^3	-0.208401	0.057537	-3.62	0.0006*

Diagnostics Plots

Residual by Predicted Plot

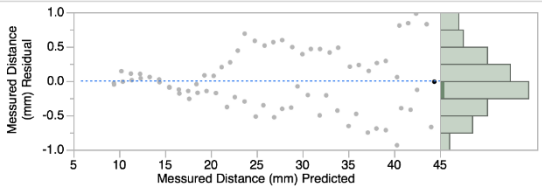

Actual by Predicted Plot

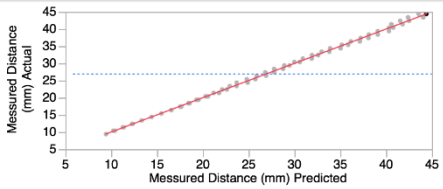

Residual by Row Plot

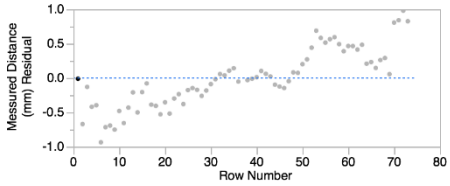

Residual by X Plot

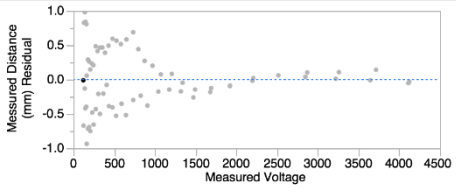

Residual Normal Quantile Plot

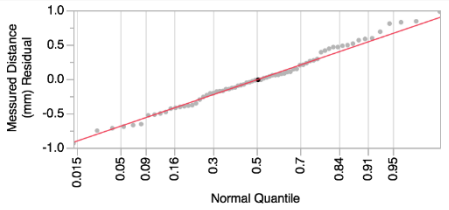

Appendix C. Mathematica Code for Sensitivity Analysis

The code below was used to run the sensitivity analysis in Mathematica. Each input was perturbed by its uncertainty value in the given in its spec sheet with all other values left at nominal. The new voltage output was compared to the nominal output to assess how sensitive the system was to these changes.

```
Clear[mvo, mvs, mmv, d, t, Oe, g, mva, Hist, S, Vs, Ang, Bo, Rg, ge, Ao, noise]
d = 31.25 (*nominal distance*)
S = .5; (*sensitivity*)
Vs = 5; (*Powers supply voltage*)
Hist = 0; (*hysteresis percentage*)
Ang = Cos[0] (*Angle in radians*)
Bo = 0; (*Bridge offset voltage*)
t = 23; (*Temperature*)
Rg = 10 000; (*Resistor value of gain resistor*)
ge = 0; (*Gain Error in amplifier*)
Ao = 0; (*Amplifier offset*)
noise = 0; (*DAQ Noise*)

(*Distance to Orsted conversion*)
Oe = 1 / ((2.0153 (d-21)^3)/10^6 + 0.0001362 (d - 21)^2 + 0.0032646 d - 0.037441)

(*Orsted to Voltage Conversion*)
mvs = Ang (Oe S Vs) + Bo + 60 Hist Vs - .001 × 60 (23 - t) Vs

(*Amplifier Gain*)
g = 80 000/Rg + 5
(*Sensor ouput to amplifier output*)
mva = Ao + mvs (g ge + g)

(*DAQ Noise*)
FinalVoltage = mva + noise
```